

Reply to the comments of the Editor

Editor Decision: Publish subject to minor revisions

Comments to the Author:

The Referees were very positive about your publication and requested only minor revisions.

I have one additional minor request which is to highlight/summarise the main assumptions made in the method in the beginning paragraphs of the paper (which are provided in detail in later in the paper) and also highlighting which parts of dynamic earth system connectivity you are and are not testing, so it is very clear to the reader what rapid attribution can and cannot provide. This no doubt will be a very well read paper.

The authors would like to thank the editor for her time and efforts. In response to the request, we have added a short description of the crucial assumptions and point the reader to Section 7, which provides the full discussion. Furthermore, we have added a few sentences of the limitations of the study.

The methodologies employed in this study are used regularly in the literature and were previously applied to the rapid attribution of the French and German 2016 flooding event (Van Oldenborgh et al. 2016) and of Storm Desmond over the UK in 2015 (Van Oldenborgh et al. 2015). The presented analysis builds upon these methodologies for event attribution and also explores the role of climate variability. We have made a few, carefully considered, crucial assumptions to facilitate the analysis. For example, these include assumptions on: the statistical distribution of 3-day precipitation in the area, the suitability of observational data and global climate models and the connection between extreme precipitation and global mean surface temperature. Please see Section 7 for a detailed discussion of all crucial assumptions and their potential impact on the results.

The present study is limited to investigation of changing precipitation statistics. Rapid attribution of flood risk was not feasible within the time frame and given our access to suitable data and models. Note that a 'climate attribution' is fundamentally different from a deterministic synoptic attribution, a detailed analysis of the chain of events that led to the extreme rainfall is not provided. The trends and internal climate variability of extreme precipitation are investigated in station observations, gridded gauge-based precipitation analysis, and high-resolution global climate model simulations. Since this paper aims to provide a first attribution assessment of the 2016 south Louisiana extreme event, we have provided a detailed data and methods section (Section 2) in which our data sets, statistical calculations for return periods and trends and data set validation methodologies are described. The rest of the paper is organized as follows: Section 3 provides observational analysis. In Section 4 we evaluate the suitability of the global climate models. Model analysis is provided in Section 5. Section 6 synthesizes our conclusions. In Section 7 we provide a detailed discussion of the crucial assumptions, further avenues of research and implications of this work.

Rapid attribution of the August 2016 flood-inducing extreme precipitation in south Louisiana to climate change

Karin van der Wiel^{1,2}, Sarah B. Kapnick², Geert Jan van Oldenborgh³, Kirien Whan³, Sjoukje Philip³, Gabriel A. Vecchi², Roop K. Singh⁴, Julie Arrighi⁴, Heidi Cullen⁵

¹Program in Atmospheric and Oceanic Sciences, Princeton University, Princeton, U.S.

²Geophysical Fluid Dynamics Laboratory (GFDL), National Oceanic and Atmospheric Administration, Princeton, U.S.

³Royal Netherlands Meteorological Institute (KNMI), De Bilt, Netherlands

⁴Red Cross Red Crescent Climate Centre, The Hague, Netherlands

⁵Climate Central, Princeton, U.S.

Correspondence to: Karin van der Wiel (kwiel@princeton.edu) or Geert Jan van Oldenborgh (oldenborgh@knmi.nl).

Abstract.

A stationary low pressure system and elevated levels of precipitable water provided a nearly continuous source of precipitation over Louisiana, United States (U.S.) starting around 10 August, 2016. Precipitation was heaviest in the region broadly encompassing the city of Baton Rouge, with a ~~three~~3-day maximum found at a station in Livingston, LA (east of Baton Rouge) from 12–14 August, 2016 (648.3 mm, 25.5 inches). The intense precipitation was followed by inland flash flooding and river flooding and in subsequent days produced additional backwater flooding. On 16 August, Louisiana officials reported that 30,000 people had been rescued, nearly 10,600 people had slept in shelters on the night of 14 August, and at least 60,600 homes had been impacted to varying degrees. As of 17 August, the floods were reported to have killed at least thirteen people. As the disaster was unfolding, the Red Cross called the flooding the worst natural disaster in the U.S. since Super Storm Sandy made landfall in New Jersey on 24 October, 2012. Before the floodwaters had receded, the media began questioning whether this extreme event was caused by anthropogenic climate change. To provide the necessary analysis to understand the potential role of anthropogenic climate change, a rapid attribution analysis was launched in real-time using the best readily available observational data and high-resolution global climate model simulations.

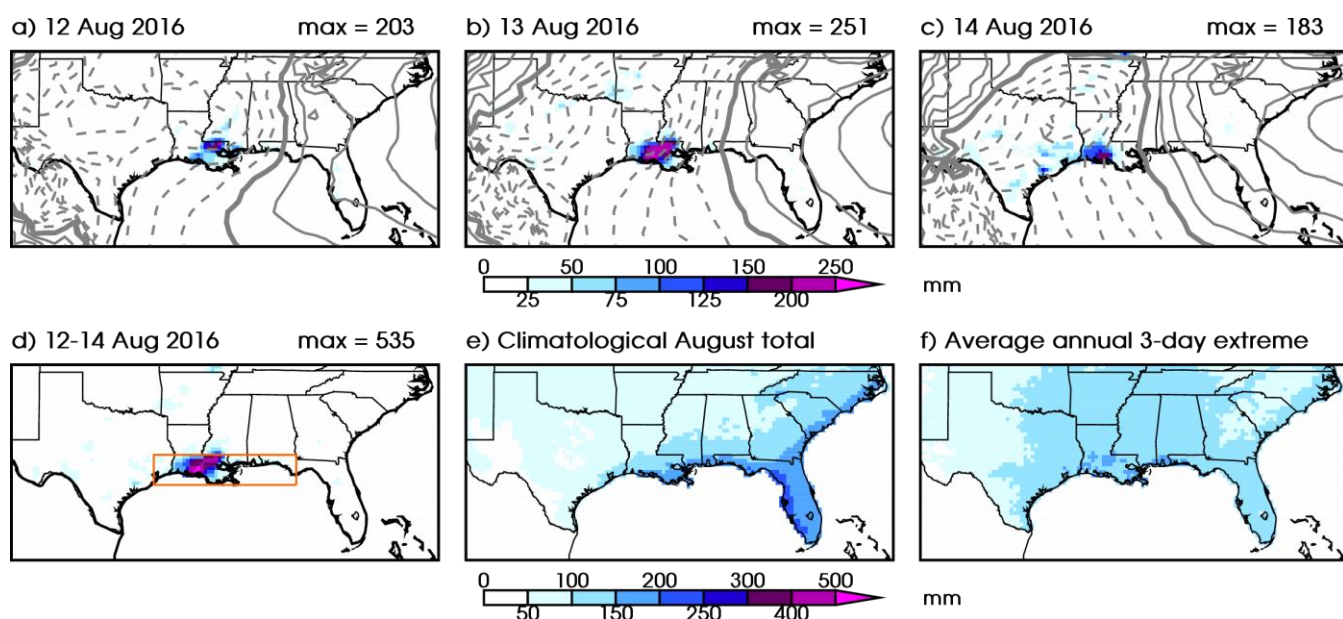
The objective of this study is to show the possibility of performing rapid attribution studies when both observational and model data, and analysis methods are readily available upon the start. It is the authors aspiration that the results be used to guide further studies of the devastating precipitation and flooding event. Here we present a first estimate of how anthropogenic climate change has affected the likelihood of a comparable extreme precipitation event in the Central U.S. Gulf Coast. While the flooding event of interest triggering this study occurred in south Louisiana, for the purposes of our analysis, we have defined an extreme precipitation event by taking the spatial maximum of annual 3-day inland maximum precipitation over the region: 29–31 °N, 85–95 °W, which we refer to as the Central U.S. Gulf Coast. Using observational data, we find that the observed local return time of the 12–14 August precipitation event in 2016 is about 550 years (95% confidence interval (C.I.): 450–1450). The probability for an event like this to happen anywhere in the region is

39 presently 1 in 30 years (C.I. 11-110). We estimate that these probabilities and the intensity of extreme
40 precipitation events of this return time have increased since 1900. A Central U.S. Gulf Coast extreme
41 precipitation event has effectively become more likely in 2016 than it was in 1900. The global climate models
42 tell a similar story, ~~in the most accurate analyses the regional probability of 3-day extreme precipitation~~
43 ~~increases by more than a factor 1.4 due to anthropogenic climate change, with the regional probability of 3-day~~
44 ~~extreme precipitation increasing due to anthropogenic climate change by more than a factor 1.4 in the most~~
45 ~~accurate analyses.~~ The magnitude of the shift in probabilities is greater in the 25 km (higher resolution) climate
46 model than in the 50 km model. The evidence for a relation to El Niño half a year earlier is equivocal, with
47 some analyses showing a positive connection and others none.

48 **1 Introduction**

49 In the second week of August, a storm system developed in the United States (U.S.) Gulf Coast region and
50 resulted in intense precipitation across south Louisiana in the region surrounding the city of Baton Rouge. The
51 highest concentration of precipitation fell over the 3-day period of 12-14 August (Figure 1a-d). Saturday, 13
52 August experienced the greatest total magnitude of precipitation and the broadest surface area of intense
53 precipitation during the storm. The National Oceanic and Atmospheric Administration (NOAA) Climate
54 Prediction Center (CPC) unified gauge-based gridded analysis of daily precipitation exhibits 25×25 km area
55 boxes with precipitation maxima reaching up to 534.7 mm (21.1 inches) over the 3-day period. In station
56 observations (a single point), a rain gauge in Livingston, LA (east of Baton Rouge) experienced an even higher
57 3-day precipitation total of 648.3 mm (25.5 inches). In places, the 3-day precipitation totals in Louisiana
58 exceeded three times that of the climatological August totals (historical average total precipitation that occurs
59 over 31-days, Figure 1e) and three times the average annual 3-day precipitation maximum (Figure 1f).

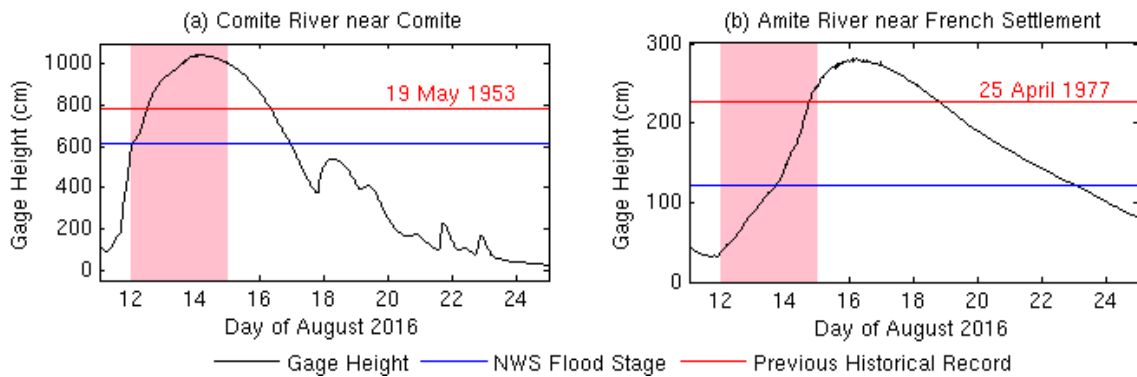
60 The intense precipitation formed due to a low pressure system that originated near Florida/Alabama on
61 5 August. At that time the National Hurricane Center stated that ~~the low pressure system it~~ might transform into
62 a tropical depression ~~after moving to the~~ ~~if it moved to the~~ Gulf of Mexico (Schleifstein 2016). Instead the
63 system remained over land and moved westward slowly. On 12 August it became near-stationary over Louisiana
64 (Figure 1a-c) allowing for the continuous development of thunderstorms in a localized area to the south and
65 southeast of the low pressure center. The stationary storm system and anomalously moist atmospheric
66 conditions (precipitable water exceeding 65 mm) created optimal conditions for high precipitation efficiencies
67 and intense precipitation rates. Though the system had a warm-core and some similarities to a tropical
68 depression, it never formed the closed surface wind circulation about a well-defined center that are needed to be
69 classified as one (National Weather Service 2016).



70

71 **Figure 1:** (a,b,c) Daily precipitation (shaded colors) and sea level pressure (grey contours, interval 1 hPa, 1015
 72 hPa contour thickened, lower contours dashed) for 12, 13 and 14 August, 2016. (d) 3-day precipitation sum 12-
 73 14 August, 2016. (e) August climatological total precipitation (1948-2015). (f) Average annual maximum 3-day
 74 precipitation event (1948-2015). Orange box in (d) shows the geographic region used for the analysis (29°-31°N,
 75 85°-95°W). Data from CPC unified gauge-based analysis of daily precipitation over the contiguous U.S. (2016
 76 data from the real time archive) and ECMWF operational analysis.

77 Historic freshwater flooding in the region encompassing Baton Rouge, Louisiana followed the extreme
 78 precipitation event. Provisional reports from 18 August, 2016 showed streamgauges managed by the United
 79 States Geological Survey (USGS) registering above flood stage levels levels at which overflow of natural banks
 80 starts to cause damage in the local area at 30 sites and found that out of 261 sites in all of Louisiana 50 were
 81 overtopped by floodwaters (Burton and Demas 2016). This was a complex event where provisional data from
 82 the USGS showed rivers responded responding to local precipitation as well as upstream and downstream
 83 conditions (Figure 2). For example, on the Comite River, a major drainage river for North Baton Rouge and its
 84 outlying districts, the provisional gauge height data exceeded the National Weather Service (NWS) flood stage
 85 from 12-16 August and even exceeded the previous height record (set 19 May, 1953). The Comite River hit its
 86 NWS flood stage level before the maximum precipitation fell in Central U.S. Gulf Coast ~~(Figure 1d)~~.
 87 Floodwaters were slow to recede due to flood stages downstream causing backwater flooding (upstream
 88 flooding caused by conditions downstream) in many neighborhoods (Burton and Demas 2016). Further
 89 downstream on the Amite River, provisional data showed that water levels exceeded the NWS floodstage from
 90 13-23 August and also exceeded the previous height record (set 25 April, 1977). Its levels declined more slowly
 91 and did not fall below floodstage until late on 23 August, due to drainage from the Comite and other tributaries
 92 upstream that hit peak floodstage days earlier (Burton and Demas 2016).



93

94 **Figure 2:** Hydrographs of gauge levels, NWS flood stage value and previous historical record for
 95 USGS station (a) 07378000 on the Comite River and (b) 07380200 on the Amite River. Shaded pink areas
 96 indicate the 3-day period of maximum precipitation (12-14 August 2016). Observed streamgauge information
 97 downloaded 25 August, 2016 from the USGS: <<http://waterdata.usgs.gov/la/nwis/uv?>>; provisional USGS data
 98 is subject to adjustment: <http://help.waterdata.usgs.gov/policies/provisional-data-statement>.

99 On 12 August the NWS issued flash flood warnings for parishes in south Louisiana, and activated the
 100 national Emergency Alert System which urged residents to move to higher ground. The Louisiana Coast Guard,
 101 National Guard, and civilian volunteers mobilized to rescue over 30,000 people from their flooded homes and
 102 cars (Broach 2016). By August 14, the federal government declared a major disaster, indicating that the severity
 103 of damage exceeded the local and state governments' combined capability to respond, initiating federal
 104 assistance for individuals and public infrastructure (Davies 2016, FEMA 2016, Stafford Disaster Relief and
 105 Emergency Assistance Act). The flooding impacted the state's agriculture industry with losses estimated in
 106 excess of \$110 million (Allen and Burgess 2016). Initial estimates also show that at least 60,600 homes were
 107 damaged, and thirteen people were killed due to the floods (Strum 2016). The American Red Cross, with FEMA
 108 and other federal and local agencies, provided shelter and emergency relief for 10,600 people initially displaced
 109 by the disaster, and the American Red Cross estimates that its ongoing relief efforts will cost \$30 million
 110 (American Red Cross 2016). To date, more than 110,000 people have registered for federal disaster assistance
 111 (FEMA, 2016). ~~FEMA has made grants totalling \$107 million available to disaster survivors for serious needs~~
 112 ~~including temporary rental assistance, and \$20 million in advance payments for National Flood Insurance~~
 113 ~~policyholders (FEMA 2016).~~

114 South Louisiana is a region where a number of phenomena can lead to flooding. For example, as a
 115 coastal region, it can experience saltwater flooding from a storm surge, when the low pressure and winds of a
 116 storm moving towards the coastline push coastal saltwater inland. This occurred in August 2005 when
 117 Hurricane Katrina impacted a broad swath of the Gulf Coast, including New Orleans, LA, with a large storm
 118 surge. Inland, precipitation can directly cause pluvial flooding by producing runoff in a region independent of a
 119 body of water (i.e. when more rain falls than can be soaked up by the ground) or fluvial flooding when water
 120 levels exceed the capacity of the river environment. For inland freshwater flooding, land surface conditions prior
 121 to an extreme precipitation event may increase the susceptibility of a region to both types of flooding, by
 122 saturating the soil (Tramblay et al. 2010, De Michele and Salvadori 2002) or increasing river levels (Pinter
 123 2006). Inland flood conditions can also be induced by water flowing through the river system after a storm due
 124 to capacity limitations, as evident along the Amite River in August 2016 (Figure 2b) due to upstream flood
 125 conditions making their way downstream. Flooding can be influenced by remote meteorological conditions as

126 river networks connect regions over vast areas. Louisiana had most recently experienced widespread inland
127 flooding in March-April 2016. Although inland freshwater flooding occurs due to a combination of the level of
128 extreme precipitation and its interaction with the land surface and river system, including human modifications
129 to those systems and responses to events, we have chosen to focus our rapid attribution study on one portion of
130 the problem: understanding the present and potentially climate change-influenced probability of extreme
131 precipitation events like the one which occurred in August 2016.

132 Synoptic forcing for precipitation extremes in the Gulf Coast region includes both mid-latitude weather
133 (cold core systems fueled by baroclinic instability), and tropical weather (warm core systems with barotropic
134 instability). Extreme precipitation has historically been classified into 3 types of events: frontal systems, tropical
135 systems, and air mass systems. Each of these categories can be further broken down; e.g. tropical systems
136 ranging from easterly waves to hurricanes, frontal systems including interactions between the polar jet and moist
137 air masses from the Gulf, squall lines, or mesoscale convective systems, and air mass systems that may include
138 heavy rainfall from upper air disturbances, or convective storms that form because of daytime heating (Keim
139 and Faiers 1996). The variety of weather systems that can give rise to precipitation extremes in the region
140 complicates the statistical analysis of the extremes and requires climate models to capture the entire distribution
141 in a realistic manner. Also, the response to radiative forcing may be non-linear: thermodynamic and/or dynamic
142 changes may be different for ~~different each~~ weather systems (O’Gorman 2015)type.

143 In this article, we analyze the historical context and changes in statistics of extreme precipitation like
144 the one experienced during August 2016 in south Louisiana by defining an extreme event by its local or regional
145 maximum 3-day precipitation. We have focused our analysis on stations or land surface grid cells in the region:
146 ~~29–31 °N, 85–95 °W~~ (illustrated by the ~~red-orange~~ box in Figure 1d), which we hereafter refer to as the “Central
147 U.S. Gulf Coast”. Here we report the results of our rapid attribution study conducted by several organizations
148 within two weeks of the event. The need for a rapid attribution study arises from the current intense public
149 discussion that results from the significant societal impacts of this particular event and a continuous general
150 interest in climate change. Media coverage following the event has linked into the growing body of scientific
151 evidence that precipitation extremes are expected to increase due to the greater moisture content of a warmer
152 atmosphere following Clausius-Clapeyron scaling (O’Gorman 2015, Lenderink and Attema 2015, Scherrer et al,
153 2016): e.g. “Disasters like Louisiana floods will worsen as planet warms, scientists warn” (Milman 2016),
154 “Flooding in the South looks a lot like climate change” (Bromwich 2016). However, specific scientific
155 statements for the event as observed in south Louisiana cannot be made based on general assessments of the
156 connection of global warming and extreme rainfall. While attribution studies at a more traditional scientific pace
157 (several months up to a year later) are important and add to scientific understanding of changing extremes,
158 reporting results recently after an extreme event may enhance the societal understanding of climate change and
159 extreme weather, and provide often requested information for management decisions following the event.

160 The methodologies employed in this study are used regularly in the literature and were previously
161 applied to the rapid attribution of the French and German 2016 flooding event (Van Oldenborgh et al. 2016) and
162 of Storm Desmond over the UK in 2015 (Van Oldenborgh et al. 2015). The presented analysis builds upon these
163 methodologies for ~~event anthropogenic climate change~~ attribution and also explores the role of climate
164 variability. We have made a few, carefully considered, crucial assumptions to facilitate the analysis. For
165 example, these include assumptions on: the statistical distribution of 3-day precipitation in the area, the

166 [suitability of observational data and global climate models and the connection between extreme precipitation](#)
167 [and global mean surface temperature. Please see Section 7 for a detailed discussion of all crucial assumptions](#)
168 [and their potential impact on the results.](#)

169 [The present study is limited to investigation of changing precipitation statistics. Rapid attribution of](#)
170 [flood risk was not feasible within the time frame and given our access to suitable data and models. Note that a](#)
171 [‘climate attribution’ is fundamentally different from a deterministic synoptic attribution, a detailed analysis of](#)
172 [the chain of events that led to the extreme rainfall is not provided.](#) The trends and internal climate variability of
173 extreme precipitation ~~is~~ **are** investigated in station observations, gridded gauge-based precipitation analysis, and
174 high-resolution global climate model simulations. Since this paper aims to provide a first attribution assessment
175 of the 2016 south Louisiana extreme event, we have provided a detailed data and methods section (Section 2) in
176 which our data sets, statistical calculations for return periods and trends and data set validation methodologies
177 are described. The rest of the paper is organized as follows: Section 3 provides observational analysis. In
178 Section 4 we evaluate the suitability of the global climate models. Model analysis is provided in Section 5.
179 Section 6 synthesizes our conclusions. In Section 7 we provide a detailed discussion of crucial assumptions and
180 their potential impact on the results, further avenues of research and implications of this work.

181 **2 Data and methods**

182 **2.1 Observational data**

183 We utilize both point station observations and gridded analysis in this paper. The point station data are from the
184 Global Historical Climatology Network daily product (GHCN-D) version 3.22 (Menne et al. 2012, 2016). The
185 data set provides daily observations for stations worldwide. Data is quality controlled before becoming available
186 in near-real time. Inside the defined Central U.S. Gulf Coast (Figure 1d), 324 stations with a minimum of 10
187 years of data are available for the period 1891 to present (August 2016). However, not all stations provide data
188 for the entire period, and spatial proximity between stations means that not all data points provide independent
189 information ([see Section 7.1](#)). Therefore for some analyses a smaller selection of the available stations is taken
190 into account. Selection criteria are described in the relevant sections.

191 The gridded analysis used here is the product of the NOAA ~~Climate Prediction Center (CPC)~~ **CPC**
192 Unified Gauge-Based Analysis of Daily Precipitation over the contiguous U.S. (Higgins et al. 2000). The data
193 set interpolates point station data on a $0.25^{\circ} \times 0.25^{\circ}$ uniform latitude-longitude grid, based on the optimal
194 interpolation scheme of Gandin and Hardin (1965). The CPC dataset covers the period 1 January 1948 to
195 present (August 2016), data from 2007 onwards has been made available in real time. Because this is a gridded
196 product, daily precipitation sums represent an areal average ($0.25^{\circ} \times 0.25^{\circ}$) rather than a point measurement.
197 Therefore precipitation extremes are expected to be of smaller magnitude in the gridded product (Chen and
198 Knutson 2008), as was noted for the south Louisiana event above (3-day total maxima of 534.7 mm in the CPC
199 gridded versus 648.3 mm in the point station data). The gridded analysis and the individual station data are not
200 independent, as the precipitation station data is the underlying source for the gridded analysis; consequently,
201 changes in gauge station density in space and time (as discussed above for GHCN-D) also impact the gridded
202 analysis. We note that, for comparisons with climate models - in which precipitation represents area averages,

203 and not point values - the area-averaged precipitation values from the gridded analysis are likely more
204 meaningful for comparison with models than point station data (Chen and Knutson 2008, Eggert et al, 2015).

205 We use the National Aeronautics and Space Administration (NASA) Goddard Institute for Space
206 Science (GISS) surface temperature analysis (GISTEMP, Hansen et al. 2010) for estimates of the development
207 of global mean surface temperature over time. This gridded data set is based on the GHCN point station data
208 over land, NOAA Extended Reconstructed Sea Surface Temperature (ERSST, Huang et al. 2015) version 4 over
209 oceans and Scientific Committee on Antarctic Research (SCAR) point station data for Antarctica.

210 **2.2 Model and experiment descriptions**

211 Many of the meteorological phenomena that cause extreme precipitation at the [Central U.S.](#) Gulf Coast are
212 small-scale, therefore only high-resolution models can simulate them realistically. We verified that the Royal
213 Netherlands Meteorological Institute (KNMI) EC-Earth 2.3 T159 experiments (~150km, Hazeleger et al. 2012)
214 and the United Kingdom (U.K.) Met Office HadGEM3-A N216 (~60km, Christidis et al. 2013) models do not
215 realistically represent precipitation extremes in the region.

216 We therefore use two higher-resolution global climate models in our analysis from the NOAA
217 Geophysical Fluid Dynamics Laboratory (GFDL). Both models were developed from the GFDL Coupled Model
218 version 2.1 (CM2.1, Delworth et al. 2006) using a cubed-sphere finite volume dynamical core (Putman and Lin
219 2007) with 32 vertical levels. Atmospheric physics are taken from the GFDL Coupled Model version 2.5
220 (CM2.5, Delworth et al. 2006, 2012). The two models share the same ocean and sea ice components with a 1°
221 horizontal resolution, but differ in their atmosphere and land horizontal resolution. In the Forecast-oriented Low
222 Ocean Resolution model (FLOR, Vecchi et al. 2014), there are 180 points along each cubed-sphere finite
223 volume dynamical core face (FV3-C180), which relates to a resolution of 0.5° per cell along the Equator. This
224 has been interpolated to a 0.5°×0.5° uniform latitude-longitude grid. In the high-resolution version of the model
225 (HiFLOR, Murakami et al. 2016), there are 384 points along each face (FV3-C384) on the cubed-sphere finite
226 volume dynamic core, which relates to a resolution of 0.23° per cell along the Equator. This has been
227 interpolated to a 0.25°×0.25° uniform latitude-longitude grid. For FLOR we use a flux-adjusted version of the
228 model (FLOR-FA), in which atmosphere-to-ocean fluxes of momentum, enthalpy and freshwater are adjusted to
229 bring the simulated fields closer to their observed climatological state. [This procedure reduces model biases of
230 for example SSTs, tropical cyclones \(Vecchi et al. 2014\) and precipitation patterns. We assume the modeled
231 response to changes in radiative forcing are not impacted by the flux-adjustment \(see Section 7.1\).](#) The
232 adjustment method is described in detail in Vecchi et al. (2014). Descriptions on how to access the data used in
233 this study are provided in the Data Availability section.

234 Table 1 describes six different global coupled model experiments that have been performed using
235 FLOR-FA and HiFLOR, which —for each model— differ in the type of radiative forcing that is prescribed, thus
236 allowing us to assess the impact of radiative forcing on the statistics of weather extremes in these models. With
237 FLOR-FA there are two sets of experiments. First, we made use of a multi-centennial integration in which
238 values of radiative forcing agents (solar forcing, anthropogenic and natural aerosols, well-mixed greenhouse
239 gases, ozone, etc.) are prescribed to remain at levels representative of a particular time - the mid-19th century in
240 this case (Jia et al. 2016); radiative forcing agents are prescribed at the 1860 values following the protocol of the
241 Fifth Coupled Model Intercomparison Project (CMIP5, Taylor et al. 2009). These types of experiments with

242 global climate models are often referred to as “control” experiments (“pre-industrial control” in this particular
 243 case) but here we label this class of experiments as “static radiative forcing” experiments, since with HiFLOR
 244 we fix radiative forcing at a number of levels. In the static radiative forcing experiments the years of the
 245 integration bear no relation to the real world calendar. The second set of experiments with FLOR-FA is a suite
 246 of five realizations (or “ensemble members”) in which the radiative forcing is prescribed to follow estimates of
 247 past and future radiative forcing changes over the period 1861-2100 (Jia et al. 2016); the forcing agents for the
 248 period 1861-2005 are prescribed to follow the CMIP5 historical experiment protocol, and for the period 2005-
 249 2100 they follow the CMIP5 Representative Concentration Pathway 4.5 (RCP4.5), which represents the medium
 250 range greenhouse gas emissions scenario (Van Vuuren et al. 2011). The five realizations of 1861-2100
 251 experiments differ only in their initial conditions on January 1, 1861, which are taken from five different years
 252 from the long FLOR-FA preindustrial static forcing experiment. In these experiments, the calendar of the
 253 experiments is connected to the history of radiative forcing - but the internal climate variations (e.g., El Niño
 254 events) and weather fluctuations (e.g., individual storms) are not constrained to follow their observed sequence.
 255 The static climate experiment has a slow drift because the slow climate components, notably the deep ocean,
 256 were not in equilibrium at the beginning of the run, this is most noticeable in the first 1000 years of the
 257 integration.

258

259 **Table 1:** Global coupled model experiments performed with the FLOR-FA and HiFLOR models.

Model	Type of forcing	Representative year of forcings	No. of ensembles	No. of modeled years in total
FLOR-FA	Static radiative forcing	1860	1	3550
FLOR-FA	Time-varying radiative forcing	1861-2100	5	1200 (5 realizations of 240 years)
HiFLOR	Static radiative forcing	1860	1	200
HiFLOR	Static radiative forcing	1940	1	75
HiFLOR	Static radiative forcing	1990	1	300
HiFLOR	Static radiative forcing	2015	1	70

260

261 With HiFLOR, there are four experiments to explore the climate sensitivity of the statistics of weather
 262 events through static radiative forcing experiments at levels representative of particular times: preindustrial
 263 conditions (fixed at 1860 values), mid-20th Century (fixed at 1940 values), late-20th Century (fixed at 1990
 264 values), and early 21st Century (fixed at 2015 values). The value of radiative forcing agents in these experiments
 265 is prescribed from either the CMIP5 Historical Forcing protocol (for the 1860, 1940 and 1990 static forcing
 266 experiments) or from the CMIP5 RCP4.5 protocol (for the 2015 static forcing experiment); and the coupled
 267 atmosphere-land-ocean-sea ice state of the model is left to evolve freely. These simulations have been integrated
 268 for different lengths of time (Table 1, last column), over which they generate their own climate under the fixed
 269 forcing; longer integrations allow us to better estimate the statistics of climate extremes, but these were the
 270 lengths of integrations available as of 15 August, 2016.

271 There are many fewer model years available with HiFLOR than FLOR-FA because the HiFLOR model
 272 was developed more recently, and because the HiFLOR model is substantially more computationally intensive
 273 (~6× the computer resources required for one year of integration) than FLOR-FA. The four HiFLOR static
 274 forcing experiments are initialized from the same ocean, atmosphere, land and sea ice initial conditions, which
 275 are representative of the observed state in the late 20th century, and the four experiments are not in radiative
 276 balance through the length of integration (the 1860 experiment has a negative top of atmosphere balance, while

277 the 1940, 1990 and 2015 experiments have positive balances). Therefore these static climate experiments each
 278 exhibit an initial rapid (~20 year) adjustment away from the late-20th century observed initial conditions, and a
 279 slower climate drift reflecting the top of atmosphere imbalance over the length of the integration. We exclude
 280 the first twenty years of each integration from our analysis, and assume (see Section 7.1) that the impact of the
 281 slow climate drift in each model experiment on the statistics of precipitation extremes is small (see justification
 282 in Section 7.1).

283 In addition to the coupled model experiments discussed above, in which the history of sea surface
 284 temperatures (SSTs) in the models emerges from the dynamics of the models and the changes in radiative
 285 forcing, for HiFLOR a set of variable forcing experiments were run over 1971-2015 in which the model is
 286 constrained by both historical radiative forcing and the observed history of monthly SST (Table 2). These
 287 experiments can be used to connect the statistics of rainfall extremes to the detailed history of SSTs that
 288 occurred over the past 45 years, part of which was a response to radiative forcing changes and part of which
 289 emerged from internal climate variations. Furthermore by construction, these experiments have a substantially
 290 smaller SST bias than the free running versions of HiFLOR, as the statistics of weather extremes and their
 291 connection to larger-scale climate can be substantially affected by SST biases (e.g. Vecchi et al. 2014;
 292 Krishnamurthy et al. 2015; Pascale et al. 2016). These experiments are described in more detail in Murakami et
 293 al. (2015) and Van der Wiel et al. (2016). The model SST was restored to the interannually varying observed
 294 field (SST_T) Met Office Hadley Centre SST product (HadISST1.1, Rayner et al. 2003) by adding an extra term
 295 to to the modeled SST tendency:

$$296 \quad \frac{dSST}{dt} = 0 + \frac{1}{\tau}(SST_T - SST) \quad \text{Eq. (1)}$$

297 with τ the restoring time scale (three ensemble members were produced with $\tau = 5$ days, three with $\tau =$
 298 10days).

299

300 **Table 2:** Restored SST experiments performed with the HiFLOR model.

Model	Type of forcing	Representative year of forcings	No. of ensembles	No. of modeled years in total
HiFLOR	Time-varying radiative forcing (CMIP5 Historical and RCP4.5); SSTs restored to observed monthly observations	1971-2015	6	270 (6 realizations of 45 years)

301 2.3 Defining an extreme event and its statistics

302 To classify the August 2016 south Louisiana flooding event, we must choose a definition for the event to guide
 303 our statistical analysis of observations and model experiments. We have chosen to classify extremes using
 304 multi-day averaged precipitation rather than single-day precipitation, to reflect the aspects of the event that
 305 resulted in the flooding of several rivers in the area. The following steps are taken to calculate our event
 306 statistics in the model and observations.

307

- 308 1. We create 3-day precipitation averages in station points/grid cells over land found in the Central U.S.
 309 Gulf Coast: 29–31 °N, 85–95 °W, which has a relatively homogenous average precipitation extreme
 310 magnitude (Figure 1f). This provides us with, for each point in space, 365 values per year (366 in leap

- 311 years) for each station point/grid cell, except the last and first years in the record when there are 364
 312 values per year (365 in leap years), since the first January 1 and last December 31 are dropped.
- 313 2. We then, at each point in space, calculate the annual maximum for each year and define it as the local
 314 extremum for the year to create a set of extreme values for further analysis.
 - 315 3. For some analyses we then take the maximum over the [Central U.S. Gulf Coast](#) region. We have
 316 carefully documented in the main text when this is the case.
 - 317 4. In the static forcing model experiments, we disregard the first 20 years of data to allow for some initial
 318 spin-up of the model in each new static forcing state.

319

320 In order to estimate the observed return periods using the 3-day annual events found above, we fit the
 321 resulting data to a Generalised Extreme Value (GEV) Distribution (Coles 2001) in a similar manner as
 322 previously done for rapid attribution of the 2015 storm Desmond over the UK (Van Oldenborgh et al. 2015) and
 323 for the rapid attribution of the 2016 flooding in France and Germany (Van Oldenborgh et al. 2016). We first
 324 analyze the GEV distribution of observations and model simulations to determine if they represent the statistics
 325 of ~~summertime~~ extreme precipitation events sufficiently to employ them in further work. To account for
 326 possible changes due to anthropogenic climate change over time, we scale the distribution with the 4-year
 327 smoothed global mean temperature (GISTEMP for observational analysis, modeled global mean 2m air
 328 temperature for model analysis), a measure of the uniform global climate response to forcing. The GEV function
 329 is represented by:

$$\begin{aligned}
 330 \quad F(x) &= \exp \left[- \left(1 + \xi \frac{x-\mu}{\sigma} \right)^{1/\xi} \right], & \text{Eq. (2)} \\
 331 \quad \mu &= \mu_0 \exp \left(\frac{\alpha T'}{\mu_0} \right), \\
 332 \quad \sigma &= \sigma_0 \exp \left(\frac{\alpha T'}{\mu_0} \right).
 \end{aligned}$$

333 Where μ is the location parameter, σ is the scale parameter, and ξ represents the shape parameter of the curve.
 334 The ratio of σ/μ reduces to the constant σ_0/μ_0 . The fit is estimated using a maximum likelihood method where
 335 σ, μ_0, σ_0 and ξ are varied. There is a penalty term on ξ : a Gaussian with a width of 0.2 is added to the likelihood
 336 function such that values larger than ~ 0.4 are penalized as unphysical. This is mainly used to restrain fits to the
 337 1000-member non-parametric bootstrap that is used to estimate uncertainty. All years are assumed to be
 338 independent for this analysis, however correlations between proximate stations or ensemble members (when
 339 available) are taken into account with a moving block [bootstrap](#) technique ([Efron and Tibshirani 1998](#)). The
 340 average number of dependent stations will be noted in the analysis.

341 The GEV is first estimated for observational data to provide a baseline for validation. We then evaluate
 342 the individual models by assessing the extent to which the GEV fit parameters (μ, σ and ξ) are similar to those
 343 fitted to the longest available observational analysis (GHCN-D). As in Van Oldenborgh et al. (2016),
 344 multiplicative bias correction is employed for the model data, which tends to improve the similarity of the GEV
 345 fit from the model and the observations.

346 After a conditional GEV fit has been computed, with global mean surface temperature as the covariate,
 347 Eq. (2) can be inverted to find the probability of the south Louisiana event in any year. We thus estimate the
 348 probability for the south Louisiana event in 2016, p_1 , and its probability in some earlier year, p_0 - taken as [1860](#),
 349 1900 or the first year with available data if that is later. ~~This~~ ~~year~~ ~~1900~~ is taken as representative for a climate

350 that has not yet been strongly influenced much by anthropogenic climate change. The probabilities for an event
351 with a magnitude at least as great as that observed in south Louisiana in each year, i , can be expressed as return
352 times, τ_i , by:

$$353 \quad \tau_i = 1/p_i \quad \text{Eq. (3)}$$

354 The ratio of probabilities or return periods from different years is known as the risk ratio where:

$$355 \quad RR = p_1/p_0 = \tau_0/\tau_1 \quad \text{Eq. (4)}$$

356 The risk ratio is a measure of how the likelihood of an event has changed in the target year (*e.g.*, 2016) versus a
357 reference year (*e.g.*, 1900). A RR value of 1 would mean that the likelihood has not changed in the baseline year
358 versus the target year. This ratio is therefore an indicator of changes in likelihood, but alone it cannot attribute
359 this difference to a given mechanism.

360 There are multiple methods available to evaluate the impact of radiatively-forced climate change on the
361 change in likelihood of events. For FLOR-FA, we repeat the analysis for the observations using data from the
362 transient experiments. The natural variability from an ensemble member of the model is uncorrelated with that
363 of other ensemble members, or the real world, so common changes in the ensemble members are therefore due
364 to the prescribed external forcings. Multi-decadal changes over the past century are dominated by anthropogenic
365 forcings. For the highest-resolution global climate model, HiFLOR, we fit a concatenated time series of
366 maximum precipitation and the corresponding global mean temperatures from the four static forcing
367 experiments to Eq. (2). Furthermore, in HiFLOR we fit the trends in extremes in the variable forcing 6-member
368 ensemble covering 1971-2015. These simulations feature restored SSTs which reduce oceanic temperature
369 biases compared to a fully free running ocean component and include the same oceanic variability as the real
370 world (*e.g.* El Niño events, North Atlantic decadal variability).

371 We use the same procedure to investigate the effect of ENSO on extreme precipitation on the U.S.
372 Central Gulf Coast, replacing the smoothed global mean temperature by an index of the strength of El Niño as
373 covariate in Eq. (2). As the 2016 flooding occurred half a year after a strong El Niño event, we take as an index
374 a detrended version of the Niño3.4 index with a lag of six months. The detrending is done by subtracting the
375 average SST over 30 °S–30 °N.

376 **3 Observational analysis**

377 We here describe the character of the statistical distribution of observed precipitation extremes and their trends
378 in the GHCN-D point station data and the CPC gridded analysis by fitting to a time-dependent GEV distribution
379 (described in Section 2.3). Due to the many different meteorological phenomena that can lead to precipitation
380 extremes in the Central U.S. Gulf Coast, we assess the extent to which the GEV gives a satisfactory description
381 of the underlying data. We frame the results around measures of the probability per year of an event at least as
382 intense as the 2016 south Louisiana event (expressed as a return time), and the change of return time from the
383 beginning of the dataset to present (risk ratio). These return times can be assessed at a local scale (the expected
384 wait time for an event *at a particular place*) or at a regional scale (the expected return time for an event
385 *somewhere* in the Central U.S. Gulf Coast). Because the spatial scale of the most extreme precipitation events is
386 substantially smaller than the whole region, the local return times are longer than the regional return times. This
387 observational analysis on its own is only able to detect whether a trend is present, but cannot ascribe cause(s) to

388 these trends. Note that from here onwards we will principally report 3-day average precipitation values rather
389 than 3-day precipitation sums, unless stated otherwise.

390 **3.1 Point station data**

391 We first analyze point station data, as extremes are affected by interpolation and station density, using the
392 GHCN-D v3.22 dataset. This first analysis does not take the spatial maximum (Step 3 in Section 2.3), but
393 analyzes all stations in the region with at least 10 years of data. This gives 324 stations with 12536 station years
394 with data (Figure 3a), though it is crucial to note that they are not all statistically independent. The highest
395 observed value at these gauges in 2016 is 216.1 mm/day at Livingston, LA on 12–14 August (648.3 mm, three-
396 day sum).

397 Fitting these data to a time-dependent GEV distribution as described in Section 2.3 gives a reasonable
398 description of the data (Figure 3c,e), although the fit is shaped mainly by the lower-intensity events and the
399 highest-intensity events align closer to the lower bound. It should be noted that for each point station in the
400 dataset, on average another 18 are correlated with $r > 1/e$, so the number of degrees of freedom is much less
401 than the number of points. Overall it is surprising that all different meteorological situations that can give rise to
402 extreme precipitation (as laid out in Section 1) can be described with a single GEV function.

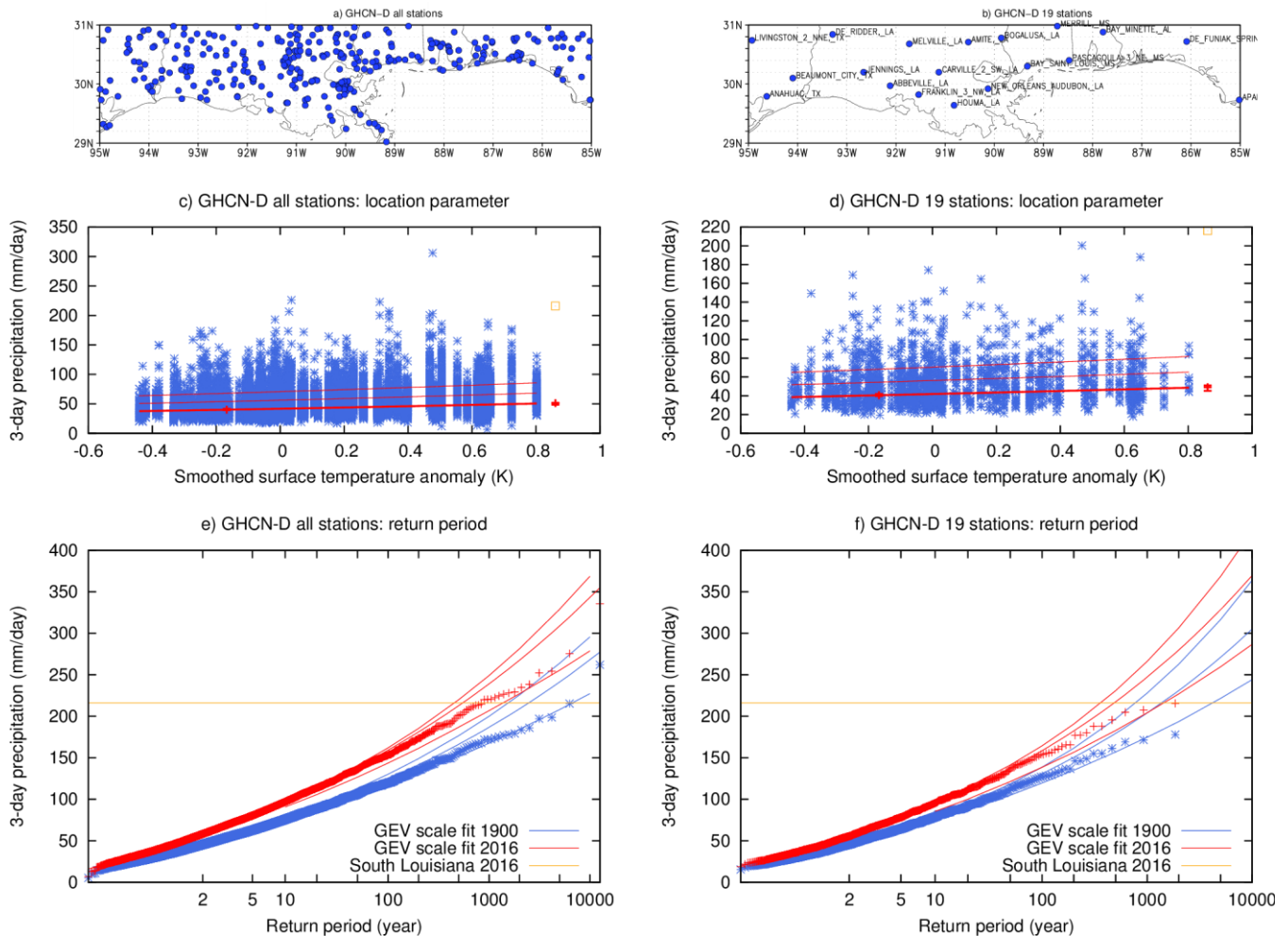
403 The local return time of a 216.1 mm/day event at a station in 2016 is about 550 yr (95% Confidence
404 Interval, C.I., 450-1450 yr). The probability of a 3-day precipitation event at a station with 216.1 mm/day or
405 more has increased by a factor 4.5 (C.I. 3.0-5.5) since 1900 in this analysis. This corresponds to an increase in
406 intensity for a given return time of 22% (C.I. 16%-22%).

407 This fit of all data available may be influenced by the spatially and temporally varying numbers and
408 locations of stations. We therefore evaluate the impact of these changes in sampling on the results by limiting
409 the analysis to stations with at least 80 years of data and at least 0.5° of spatial separation between stations. This
410 leaves 19 stations with 1849 station years (Figure 3b), which results in 2.3 stations per degree of freedom on
411 average. This analysis gives similar results: a return time of about 500 years (C.I. 360-1400) and an increase in
412 probability of a factor 2.8 (C.I. 1.7-3.8), corresponding to an increase in intensity of 17% (C.I. 10%-21%),
413 Figure 4d3d,f. The increase in probability is less than in the full station sample, although compatible within the
414 2σ uncertainties. ~~As the impact of inhomogeneities is smaller when considering longer time series, we use this
415 result from the 19 GHCN-D point stations for the trend estimate.~~

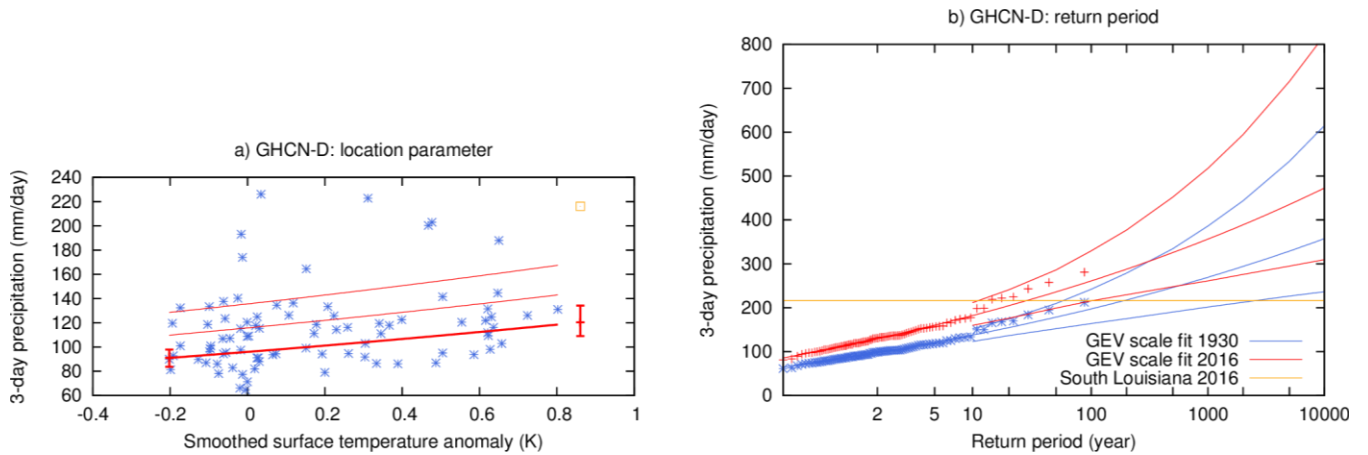
416 Our final analysis of point station data focuses on the most intense events only by considering the
417 spatial maximum of 3-day averaged precipitation anywhere in the Central U.S. Gulf Coast (Step 3 in Section
418 2.3). This answers the question how likely an event, like that of south Louisiana 2016 or worse, was anywhere
419 in the region, rather than at a specific place. In the point station data, the spatial maximum is only homogeneous
420 when the number of stations does not vary by much. We therefore again consider only those stations with at
421 least 80 years of data, but do not require a minimum distance this time. The number of stations increases up to
422 around 40 in 1950–1980 and decreases again to the present. On average 1.3 stations are correlated at $r > 1/e$ with
423 each of these stations. We consider the period 1930-2016. The decrease in number of stations at the end implies
424 that a trend in extremes will be negatively biased. The number of events is lower than before (1 per year instead
425 of 19/324 events per year), so the uncertainties are larger.

426 A fit of a time-dependent GEV to the annual and spatial maximum of 3-day averaged precipitation
 427 describes the data well (Figure 4). The return time for an event like south Louisiana 2016 anywhere in the
 428 Central U.S. Gulf Coast is currently around 30 yr (between 11 yr and 110 yr with 95% C.I.). This is a factor 6.3
 429 (C.I. 2.1-50) more than it was in the climate of 1930, corresponding to an increase of intensity of about 25%
 430 (C.I. 12%-35%).

431 Analyses of station data analogous to the ones above but for the season July-August-September (JAS)
 432 show somewhat smaller trends, but with larger error margins. The estimated ranges of the JAS analyses and the
 433 all year analyses overlap.



434
 435 **Figure 3:** Fit of the annual maximum 3-day average GHCN-D station precipitation on the Central U.S. Gulf
 436 Coast to a GEV that scales with smoothed global mean surface temperature. (a) Location of all GHCN-D
 437 stations with minimum 10 years of data, (c) observations (blue marks), location parameter μ (thick red line
 438 versus global mean temperature anomalies, relative to 1980-2010), $\mu + \sigma$ and $\mu + 2\sigma$ (thin red lines), the two
 439 vertical red lines show μ and its 95% C.I. for the two climates in (e). (e) Gumbel plot of the GEV fit in 2016
 440 (red line, with 95% uncertainty estimates) and 1900 (blue line), marks show data points drawn twice: scaled up
 441 with the trend to 2016 and scaled down to 1900. The yellow square (line) denotes the intensity of the observed
 442 event at Livingston, LA. (b,d,f) as (a,c,e) but for 19 GHCN-D stations with minimum 80 years of data and
 443 minimum spatial separation of 0.5° .



444

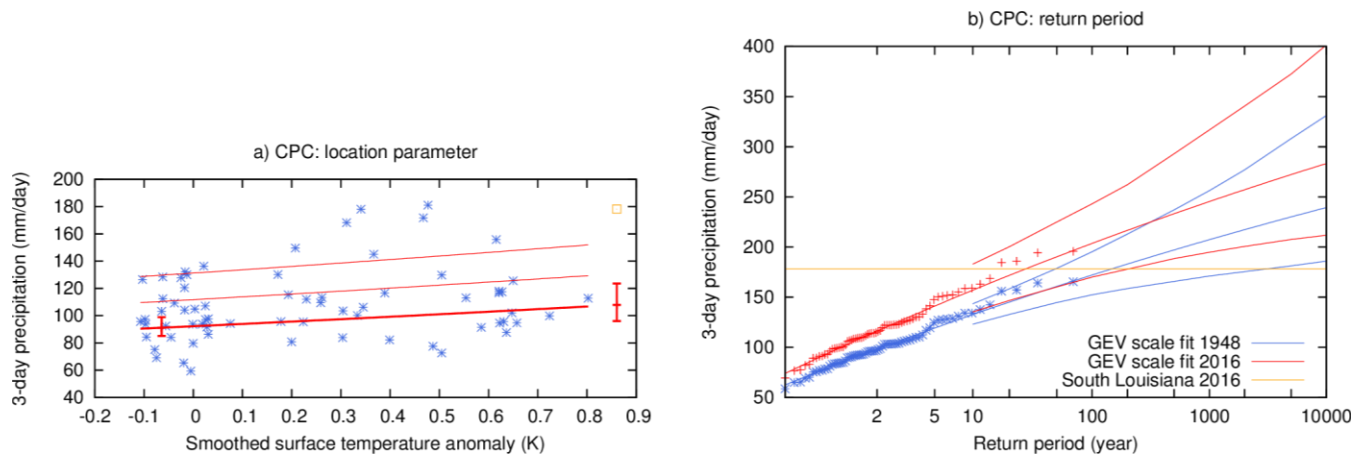
445 **Figure 4:** Fit of the spatial and annual maximum 3-day average GHCN-D station precipitation on the Central
 446 U.S. Gulf Coast to a GEV that scales with smoothed global mean surface temperature. (a) Observations (blue
 447 marks), location parameter μ (thick red line), $\mu + \sigma$ and $\mu + 2\sigma$ (thin red lines versus global mean temperature
 448 anomalies), the two vertical red lines show μ and its 95% confidence interval for the two climates in (b). (b)
 449 Gumbel plot of the GEV fit in 2016 (red line, with 95% uncertainty estimates) and 1930 (blue line), marks show
 450 data points drawn twice: scaled up with the trend to 2016 and scaled down to 1900. The yellow square (line)
 451 denotes the intensity of the observed event at Livingston, LA.

452 3.2 Gridded analysis

453 To compare with the model data, we also analysed the CPC $0.25^\circ \times 0.25^\circ$ gridded precipitation analysis 1948–
 454 2016. Because the spatial extent of 3-day averaged precipitation extremes is larger than the grid boxes, we first
 455 averaged these to a $0.5^\circ \times 0.5^\circ$ latitude-longitude grid. The highest value in 2016 is then 158.77 mm/day, which is
 456 the highest in the record. This is lower than at a single grid point due to the spatial averaging. A GEV fit of all
 457 0.5° grid points (not shown) gives a return time of 550 yr with an uncertainty from 300 to 2000 yr, compatible
 458 with the station analysis but with larger uncertainties. The probability has increased by a factor 3.5 (C.I. 2.0-11)
 459 since 1948, corresponding to an increase in intensity of 15% (C.I. 9%-24%).

460 Taking the spatial maximum of the original $0.25^\circ \times 0.25^\circ$ grid we find that the highest observed value in
 461 2016 is 178.2 mm/day on 12–14 August (534.7 mm in three days). The record is too short to draw robust
 462 conclusions from a fit of a GEV depending on global mean temperature except that the precipitation maxima
 463 also increase in this dataset (Figure 5). In this dataset, the return time for an event like 2016 anywhere on the
 464 Central U.S. Gulf Coast is currently between 9 and 200 yr (best estimate 25 yr). This is about a factor 5 (C.I.
 465 1.1-60) larger than it was around 1948, which equates to an increase in intensity for an event like 2016 of
 466 roughly 15% (C.I. 0.4%-30%).

467 As for station data, analyses of CPC similar to the ones above but for the season JAS show somewhat
 468 smaller trends, but with larger error margins. The estimated ranges of the JAS analyses and the all year analyses
 469 overlap.



470

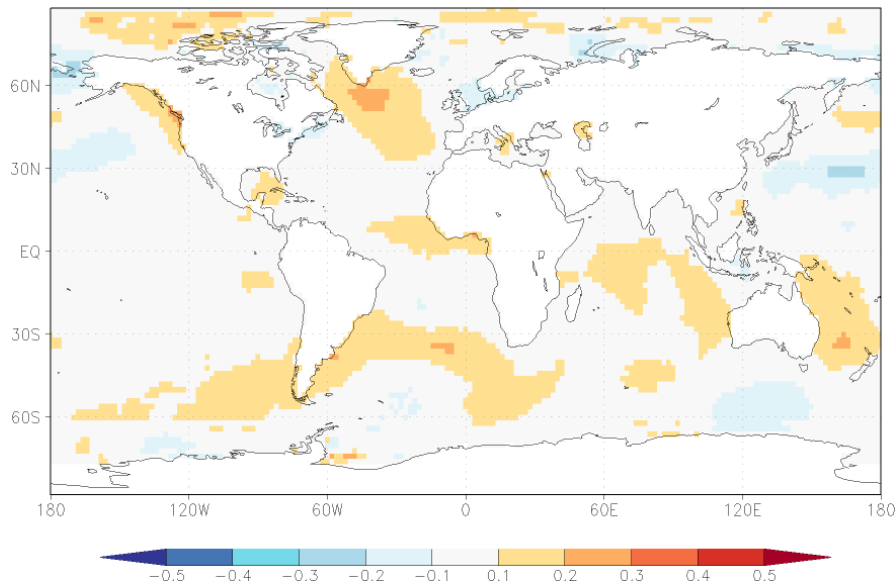
471 **Figure 5:** As Figure 4 but for the spatial and annual maximum 3-day average 1948–2016 $0.25^\circ \times 0.25^\circ$ gridded
 472 CPC analysis.

473 **3.3 Influence of natural variability**

474 We investigate the influence of natural variability on the probability of an event like south Louisiana 2016 by
 475 using indices of detrended SST as covariates in the time-dependent GEV fits. We first examine the influence of
 476 El Niño-Southern Oscillation (ENSO) by using as a covariate 6-month lagged Niño 3.4-index (5°S – 5°N , 170° –
 477 120°W) minus SST averaged of 30°S – 30°N to remove to first order the effects of global warming. This is
 478 inspired by the heavy rain events after the 1997/98 El Niño event. A comparison of recent Niño 3.4 conditions
 479 with those from a year following the strongest La Niña year (1917) in a fit of all 324 stations with more than 10
 480 years of data suggests that anomalously warm tropical Pacific SSTs significantly ($p < 0.1$) increase the
 481 probability of an event like south Louisiana 2016, but not by much. In the year after El Niño, the probability is a
 482 factor 1.3 (C.I. 1.0-1.9) higher than in a year following a very strong La Niña. However, the maximum of
 483 stations with at least 80 years, which represents the largest events, does not show a signal, albeit with a large
 484 uncertainty of a factor 0.5 decrease to a factor 1.7 increase.

485 Simultaneous correlations with global SSTs indicate a region in the North Atlantic that has a significant
 486 relationship with Central U.S Gulf Coast extreme precipitation at $p < 0.1$ (Figure 6). Although the field
 487 significance is very low, the region is a well-known source of decadal variability and predictability (e.g.,
 488 Hazeleger et al. 2013), so we still consider it a possible source of decadal variability of extreme precipitation.
 489 We use an area-average of SSTs between 45°N – 60°N and 50°W – 20°W as a covariate in the GEV fit. The region was
 490 anomalously cold in 2016, so we compare the changed probability with a warm year (2006). In this statistical
 491 analysis, North Atlantic SSTs are significantly correlated ($p < 0.01$) to Central U.S Gulf Coast precipitation (by
 492 design, as we chose the region that has a significant correlation), with recent below average SSTs decreasing the
 493 probability of an event like 2016 (risk factor 0.37, C.I. 0.11-0.81). To ascertain whether this is a physical
 494 connection and not just a coincidence by picking the region of largest correlations, we need to analyse model
 495 results.

496



497
 498 **Figure 6:** Correlation coefficient between Central U.S. Gulf Coast spatial and annual maximum of 3-day
 499 extreme precipitation intensity and annual mean SST (ERSST v4) with a linear regression on the global mean
 500 temperature removed at each grid point.

501 **4 Model evaluation**

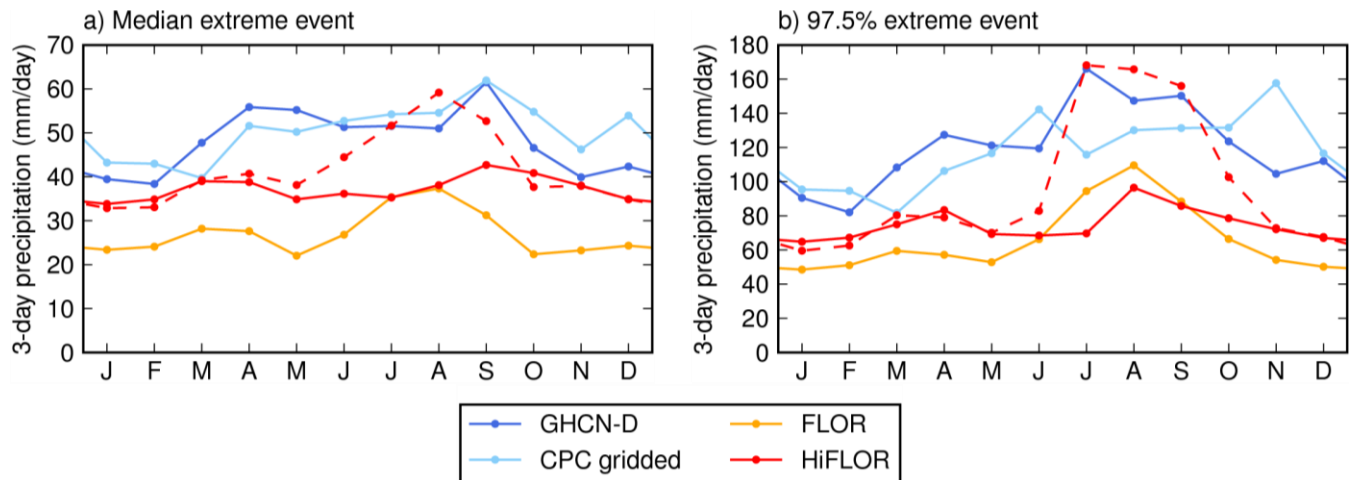
502 We here describe an evaluation of simulated precipitation extremes in the two global coupled models (model
 503 descriptions in Section 2.2). Precipitation is a notoriously difficult field to simulate, as many coupled climate
 504 models exhibit large biases (Dai 2006, Flato et al. 2013). Though FLOR-FA and HiFLOR underestimate the
 505 intensity of Central U.S. Gulf Coast precipitation extremes slightly, this bias is significantly reduced in these
 506 high-resolution models compared to standard-resolution models (Van der Wiel et al. 2016).

507 **4.1 Annual cycle and intensity**

508 First we analyse the annual cycle of extreme precipitation intensity. We consider the median and 97.5 percentile
 509 of the monthly maximum of the spatial maximum of 3-day averaged precipitation (Figure 7). The 97.5
 510 percentile events are of smaller magnitude than the south Louisiana observed event (100-150 mm/day versus
 511 200 mm/day), but we consider smaller magnitude events to increase the number of events in the calculation and
 512 hence decrease uncertainties.

513 The observed precipitation extremes in spring and summer are generally more intense than in autumn
 514 and winter (Figure 7a). There is no agreement between the two observational products on which season sees the
 515 most intense precipitation extremes (97.5 percentile, Figure 7b), though extremes in March-October are more
 516 intense than in winter. This period of stronger extremes is longer than the hurricane season, which provides a
 517 fraction of these extremes. In this region, the models underestimate the intensity of extreme precipitation, which
 518 was also noted in Van der Wiel et al. (2016). FLOR-FA has a peak season for extreme precipitation intensity in
 519 JAS which is not found in the observational data. The HiFLOR SST-restored experiment, in which global SST
 520 biases are decreased compared to the free running experiments, shows a similar peak in JAS. The HiFLOR 1990

521 static forcing experiment however, doesn't show this peak. Instead it has a similar annual cycle structure to the
 522 observational data, though with a smaller amplitude.
 523

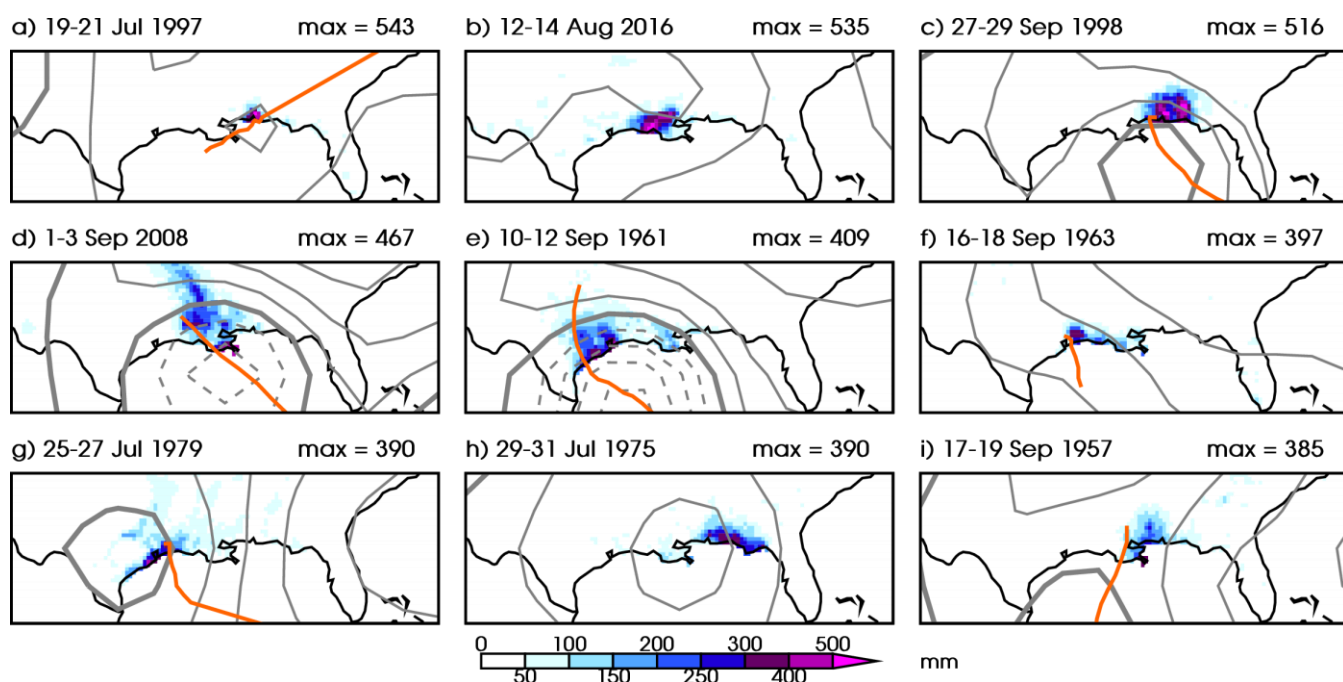


524 **Figure 7.** Annual cycle of monthly and spatial maximum 3-day averaged precipitation for point station data
 525 (GHCN-D, dark blue line), gridded observational data (CPC, light blue line) and model simulations (FLOR-FA,
 526 orange line, and HiFLOR, red lines). For HiFLOR the 1990 static forcing experiment (solid red line) and the
 527 variable forcing SST-restored experiment (dashed red line) are included. Shown are (a) the median value of the
 528 monthly extremes and (b) the 97.5 percentile.
 529

530 4.2 Meteorological conditions

531 Next, we investigate the meteorological conditions generating extreme precipitation events in both models and
 532 compare these to the observed ones. For this analysis we consider the longest static forcing experiments for each
 533 model: 1860 for FLOR-FA and 1990 for HiFLOR and the CPC gridded precipitation analysis. The selection of
 534 these events is limited to the region of interest (Central U.S. Gulf Coast) and the months JAS to facilitate
 535 comparison against the south Louisiana event.

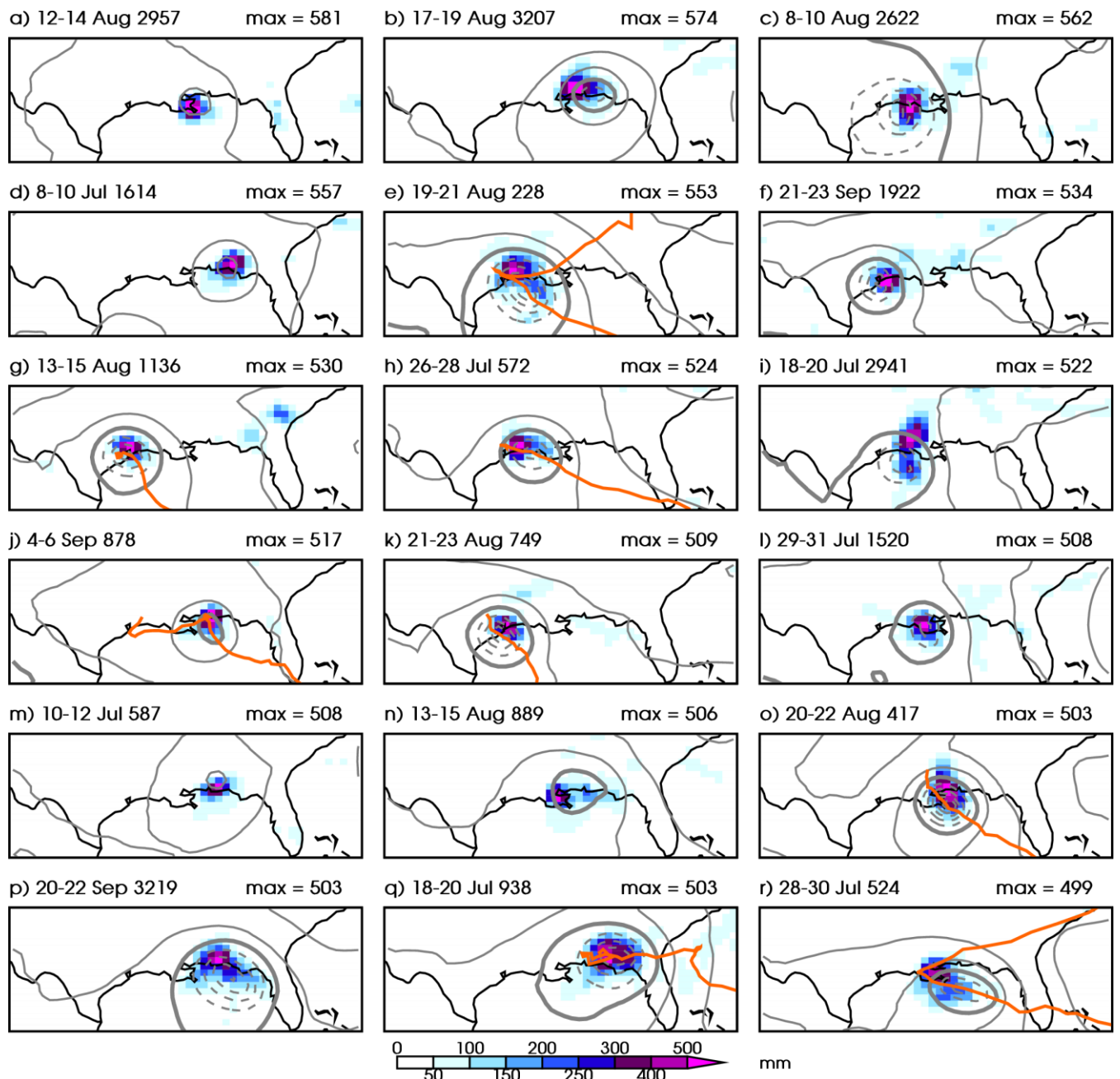
536 Precipitation totals and circulation patterns for the nine largest extreme precipitation events in the CPC
 537 analysis (JAS season only) are shown in Figure 8. Note that the 2016 south Louisiana event ranks as number 2-
 538 heavy precipitation related to Hurricane Danny in 1997 was stronger, though it was confined to a smaller area.
 539 Seven of these nine events were associated with a tropical cyclone/hurricane making landfall (78%, orange
 540 tracks are the International Best Track Archive for Climate Stewardship, IBTrACS, track estimate, Knapp et al.
 541 2010), the exceptions are July 1975 and, as noted before, August 2016. Note that the GEV analysis in Section
 542 3.2 was based on annual maxima, for which the ranked extreme events are different than the ones shown in
 543 Figure 8 (these are nine of the top 14 events when all data is taken into account, ranks 1 and 2 are the same).
 544



545

546 **Figure 8:** Top 9 extreme precipitation events in the Central U.S. Gulf Coast (29–31 °N, 85–95 °W) for the CPC
 547 gridded precipitation analysis. 3-day precipitation sum (mm, shaded colors, as in Figure 1d), 850-hPa height for
 548 the middle day (grey contours, interval 25 m, 1500 m contour thickened, lower contours dashed) from
 549 NCEP/NCAR Reanalysis 1 (Kalnay et al. 1996) and tropical cyclone track if system is classified as one (orange
 550 line, IBTrACS). These extreme events are calculated for the three month period: JAS.
 551

552 A similar figure for FLOR-FA is included as Figure 9. We now show the 18 most extreme events
 553 (approximate return period $3530/18 \approx 200$ years) in FLOR-FA. The return period in the model for these events is
 554 much larger than the return period for the observed events in the CPC analysis (approximate return period
 555 $69/9 \approx 8$ years). Despite the negative bias of precipitation extreme intensity (Section 4.1), the precipitation sums
 556 for these events are therefore larger than those in the observed data. All events are associated with a low
 557 pressure system, of which 8 (44%, orange tracks in Figure 9) are a tropical cyclone based on the TC tracking
 558 methodology of Harris et al. (2016) as implemented in Murakami et al. (2015). Note that the low pressure
 559 systems of the top 4 events do not classify as a tropical cyclone, showing the precipitation potential of non-
 560 tropical cyclone low pressure systems in the model.



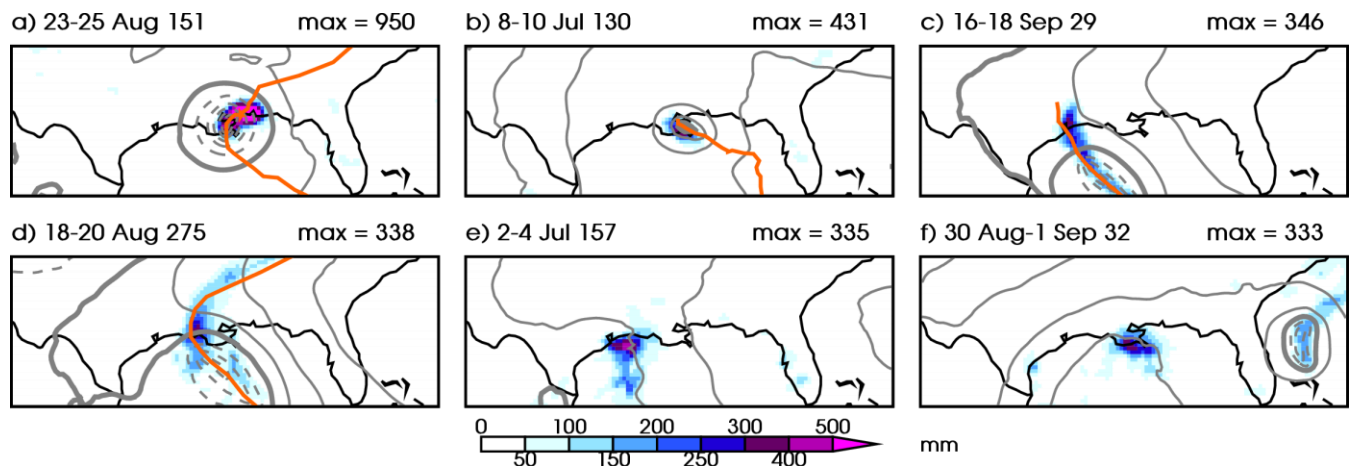
561

562 **Figure 9:** As Figure 8 but for the top 18 maximum extreme precipitation events in the 1860 FLOR-FA static
 563 forcing experiment. Note that years are model years and do not resemble dates on the real world calendar and
 564 that the model provides precipitation information over ocean grid boxes too.

565

566 Because the HiFLOR 1990 static forcing experiment is of smaller length, it is not possible to sample
 567 the 200-year return period event as was done for FLOR-FA adequately. In Figure 10 we show the 6 most
 568 extreme events (approximate return period $280/6 \approx 50$ years, the top 2 events are samples of events with return
 569 periods of about 150 years). In HiFLOR the most extreme precipitation events are the result of a tropical
 570 cyclone, though storm intensity (storms in Figure 10a,b are tropical storms, storms in Figure 10c,d are
 571 hurricanes at the time of landfall) is not related to resulting precipitation magnitude. Note that the strongest
 572 event in HiFLOR exceeds 900 mm over a 3-day period, which is much stronger than the observed values in
 573 south Louisiana.

574 In conclusion, though the precipitation extremes are of smaller magnitude in both models and the
 575 annual cycle in observations is not recovered well (Section 4.1), the meteorological system leading to these
 576 precipitation extremes in JAS are realistic and resemble observed systems (Section 4.2).



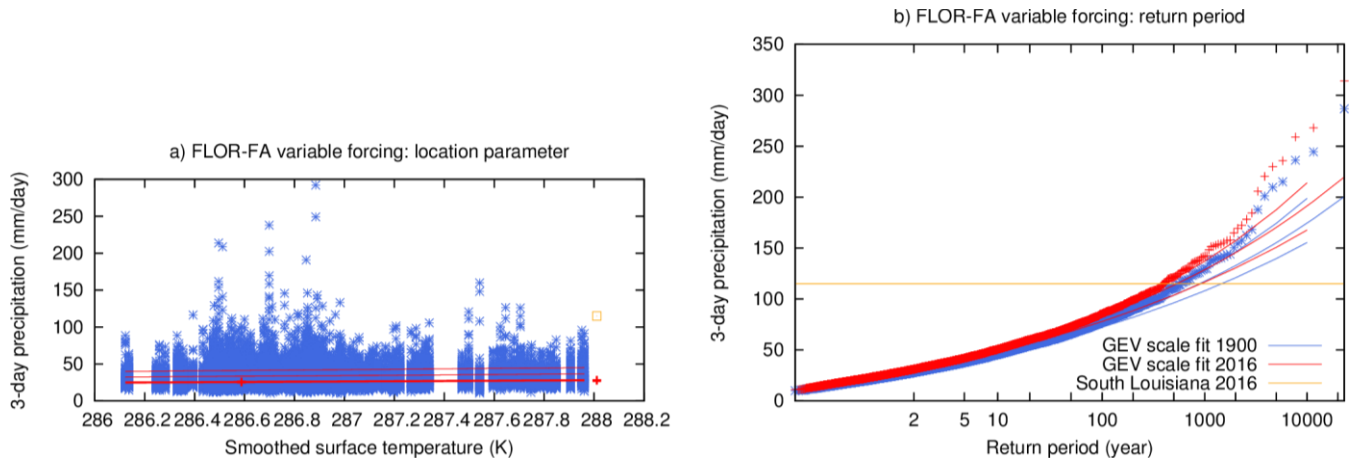
577 **Figure 10:** As Figure 8, but now for the top 6 maximum extreme precipitation events in the 1990 HiFLOR static
 578 forcing experiment. Note that years are model years and do not resemble dates on the real world calendar and
 579 that the model provides precipitation information over ocean grid boxes too.

581 5 Model analysis

582 In order to attribute the observed trend to external forcing we use global climate models that isolate the different
 583 forcings. The model and experimental description can be found in Section 2.2.

584 5.1 FLOR-FA

585 A fit of all land grid boxes ($0.5^\circ \times 0.5^\circ$, 23095 data points) to a time-dependent GEV distribution is shown in
 586 Figure 11. The uncertainties take into account the dependencies by moving spatial blocks of 7.7 grid points on
 587 average. In contrast to the observations (Figure 3) the distribution cannot be described with a single GEV
 588 function: the extremes with return times larger than about 100 years (80 mm/day) diverge from the fit that is
 589 determined mainly by the less extreme precipitation events. This so-called 'double population' problem results
 590 from different meteorological mechanisms for extreme events. We therefore cannot use this fit for attribution.



591
 592 **Figure 11:** As Figure 4 but for the annual maximum 3-day average precipitation in the FLOR-FA variable
 593 forcing experiment (based on complete experiment, 1861-2100).

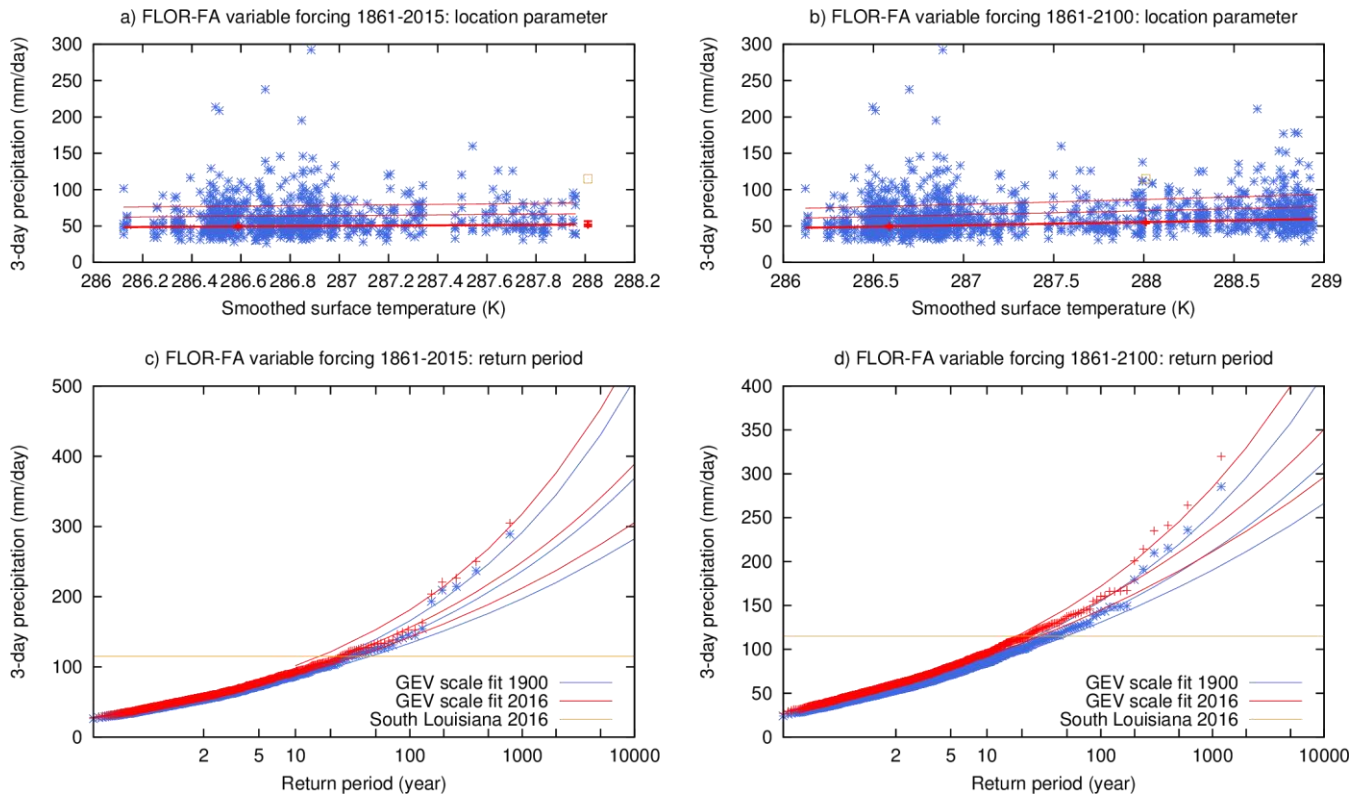
594

595 Taking the spatial maximum of all grid boxes selects only the high end of the distribution. Figure 12a,c
 596 shows the GEV fit to these extremes using data for simulated years 1861-2015. The fit is still not completely
 597 satisfactory as the highest five events (all in the early years of the experiments) fall on the upper boundary of the
 598 95% C.I. around the fit to the rest of the distribution. Due to this, the shape parameter ξ and scale parameter σ of
 599 the GEV distribution are higher than they are in the observations. Because of model bias, we define our event to
 600 have the same return period as the gridded observations in 2016 adjust the model amplitude of extremes to
 601 obtain the same return time as that in observational data, of (around 30 years, ≈ 115 mm/day). This gives a trend
 602 in this model that is significantly greater than zero at $p < 0.05$ (one-sided). However, the factor 1.3 (C.I. 1.0-1.9)
 603 increase in probability, corresponding to an increase in intensity of 5% (C.I. -1%-14%), is much less than the
 604 observed one .

605 Assuming that the relationship with global mean surface temperature does not change in the model
 606 world up to until 2100, in spite of a different mix of anthropogenic forcings (greenhouse gases and aerosols), we
 607 can improve the signal-to-noise ratio of the fit by using all data in the variable forcing experiment (Figure
 608 12b,d). For the spatial and annual maximum of 3-day averaged precipitation this gives an increase in probability
 609 of a factor 1.8 (C.I. 1.4-2.0) corresponding to an increase in intensity of 11% (C.I. 7%-12%) up to now.

610 Analogous analyses but for the season JAS show similar results, although with larger error margins.
 611 We looked for an effect of ENSO in the long static forcing experiment in the same way as in the observations.
 612 This does not show any influence of El Niño averaged over the 12 months July–June preceding the year of
 613 extreme precipitation events.

614



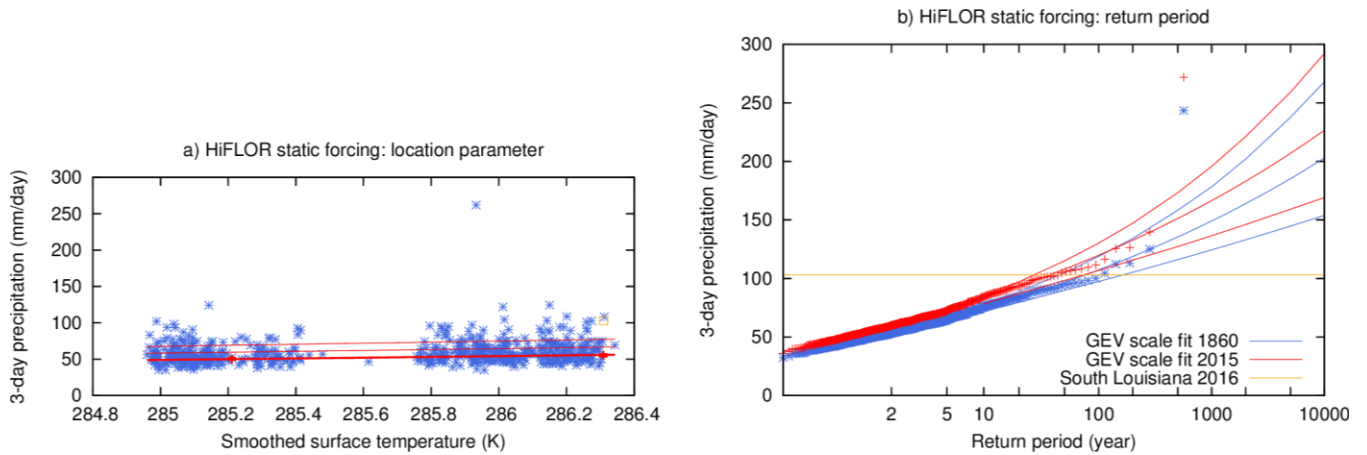
615

616 **Figure 12:** As Figure 4 but for the annual and spatial maximum 3-day average precipitation in the FLOR-FA
 617 variable forcing experiment. (a,c) taking into account years 1861-2015, (b,d) taking into account 1861-2100.

618 **5.2 HiFLOR**

619 The HiFLOR model at a higher 25 km resolution has a more realistic seasonal cycle, but underestimates extreme
 620 precipitation by 25% for a 1 in 1 year event and by 35% for 1 in 1000 year extremes. We correct for this bias ~~by~~
 621 ~~defining our event to have the same return time as the gridded observations in 2016, that is, as we did for the~~
 622 ~~FLOR-FA experiment (the 30 year event is 103 mm/day).~~ We concatenated the four static forcing experiments
 623 that we have available, leaving out the first 20 years of each, to create a 655-year record. To decrease
 624 dependencies we averaged 2×2 grid boxes into a 0.5° grid, this results in each grid box being correlated with
 625 10.3 others with $r > 1/e$ on average.

626 As was found for FLOR-FA, the GEV fit to all grid points results in a double population, therefore we
 627 disregard that analysis and instead focus on the spatial maximum precipitation extreme. Similar for FLOR-FA,
 628 taking the spatial maximum of this 50 km dataset selects mainly events in the more extreme population and does
 629 give a good fit to the GEV distribution (Figure 13). The outlier event is a tropical cyclone in the 1990 static
 630 forcing event, that was discussed in Section 4.2 (Figure 10a). The external forcing, which is the only change
 631 between the static forcing experiments, causes an increase in probability of a 103 mm or stronger event of a
 632 factor 2.0 (C.I. 1.4-2.5), in agreement with the FLOR-FA experiment up to 2100 (Figure 12b,d). This
 633 corresponds to an increase in intensity of 10% (C.I. 5%-12%).



634

635 **Figure 13:** As Figure 4 but for the annual and spatial maximum 3-day average precipitation in the HiFLOR
 636 static forcing experiments.

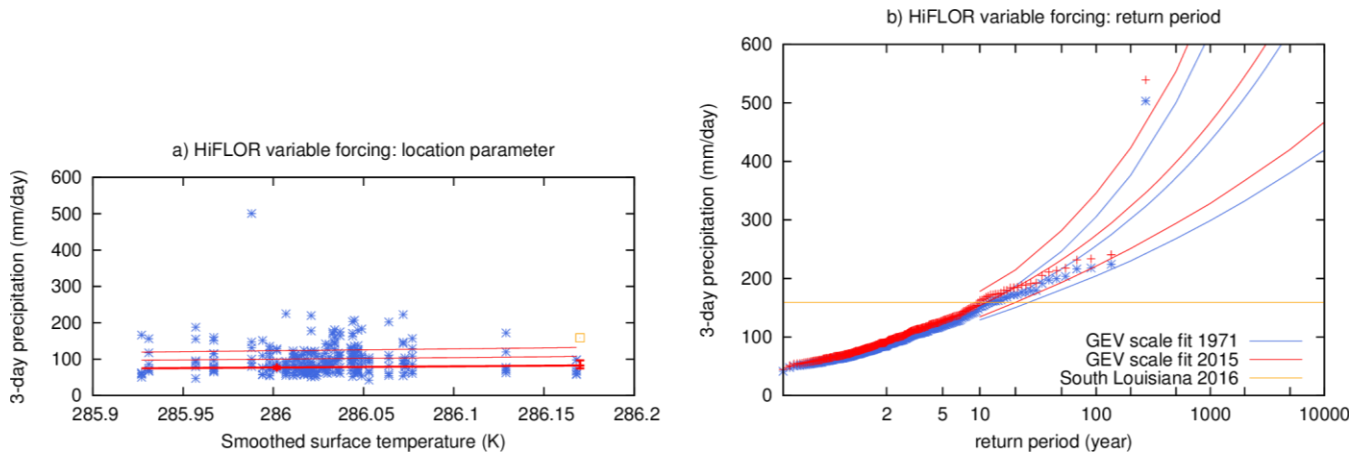
637

638 An analysis of these data using the annual averaged detrended Niño3.4 index lagged by 6 months as
 639 covariate shows a relatively strong influence of El Niño in this model, with an increase in probability from the
 640 year following strongest La Niña to the strongest El Niño of a factor about 4.2 (C.I. 1.7–6.7).

641 We followed the same procedure on the six ensemble members of the variable forcing HiFLOR
 642 experiment (1971–2015). These simulations do not have a negative bias in extreme precipitation. The restored
 643 SSTs eliminate a 2 K cold bias in the subtropical Atlantic that is present in the static forcing experiments, which
 644 may have caused the bias in precipitation extremes on the Central U.S. ~~Central~~ Gulf Coast in those simulations.
 645 Again there is one outlier event with 452.8 mm/day over three days, 1351 mm total.

646 The spatial and annual maximum of 3-day averaged extreme precipitation increases by a factor 1.8
 647 (C.I. 1.2–3.3) in these experiments over the period 1971–2015, corresponding to a change in intensity of 14%
 648 (C.I. 4%–27%), Figure 14. Although the restoring of SSTs increases the fidelity of the simulation, it also
 649 includes the non-forced natural variability of the real world, so these numbers do not isolate the forced change
 650 but show the full change including the effects of natural variability. Assuming these are small compared to the
 651 trend we can extrapolate to the full change since 1900; the period 1971–2015 only includes about 2/3 of global
 652 warming since preindustrial times. This translates to a factor 2.4 (C.I. 1.3–6) increase in probability and 22%
 653 (C.I. 6%–41%) in intensity, which is very similar to the trend found in the observational data.

654 Analyses of the season JAS show similar to somewhat smaller trends, but with larger error margins,
 655 overlapping the all-year error margins.



656

657 **Figure 14:** As Figure 4 but for the annual and spatial maximum 3-day average precipitation in the HiFLOR
 658 variable forcing restored SST experiments.

659 **6 Summary**

660 In this section we summarize the principal observational and model-based results as described in Sections 3 and
 661 5. We have analyzed two observational data products (GHCN-D point station data and CPC 0.25°×0.25°
 662 gridded analysis), to estimate the probability, and changes in probability and intensity of a 3-day precipitation
 663 event as large as that observed in south Louisiana 2015. The analysis was confined to the Central U.S. Gulf
 664 Coast (29–31 °N, 85–95 °W) and relies on time-dependent GEV fits to the data. First we investigated
 665 probabilities and changes at a single station, i.e. the probability of such an event *at a fixed place* in the region.
 666 Second we investigated regional probabilities and changes, i.e. the probability of such an event *anywhere* in the
 667 region. The spatial scale of the most extreme precipitation events is significantly smaller than the region
 668 considered, therefore the second probability is lower than the first. To attribute the observed changes to forced
 669 anthropogenic climate change, we repeat the analysis using high-resolution global climate model data from
 670 GFDL FLOR-FA and GFDL HiFLOR. GEV fits for the local analysis were unsatisfactory, therefore we only
 671 report the regional change in probabilities.

672 The expected return period of a comparable 3-day precipitation event at a single station as high as the
 673 maximum observed is 450 to 1450 year, best estimate 550 year. Return periods like these are often written as a
 674 "1 in 1000 year event". The return time for observing an event anywhere in the region is lower: between 11 and
 675 110 year (best estimate 30 years). All observational analyses found clear positive trends, with an increase in
 676 probability for the regional event of about a factor 6.3 (97.5% certain more than 2.1), and an increase in
 677 intensity of 12% to 35% (Table 3). Estimates based on CPC gridded data are comparable but have larger ranges
 678 due to the shorter period of data availability.

679 **Table 3:** Summary of observed (first two rows) and modeled (third row and down) changes in regional rainfall
 680 extremes in Central U.S. Gulf Coast. Note the modeled changes can be attributed to anthropogenic climate
 681 change.

Data source (years used for calibration)	Baseline regional return period for 2016 event (95% confidence range, observations only)	Years change calculated over	Change of return period in present day over given years (95% confidence range)	Change in intensity of regional 30- year return event in 2016 since beginning of record (95% confidence range)
GHCN-D rain	30 year (11 - 110)	1930-2016	6.3× (2.1 ... 50)	+25% (12% ... 35%)

gauges, minimum 80 year data (1930- 2016)				
CPC 0.25°×0.25° gridded data (1948-2016)	25 year (9 - 200)	1948-2016	5.4× (1.1 ... 60)	+15% (0.4% ... 30%)
FLOR-FA variable forcing experiment (1861-2015)		1900-2016	1.3× (1.0 ... 1.9)	+5% (-0.5 ... 14%)
FLOR-FA variable forcing experiment (1861-2100)		1900-2016	1.8× (1.4 ... 2.0)	+11% (7% ... 12%)
HiFLOR static forcing experiment (1860, 1940, 1990, 2015)		1860-2015	2.0× (1.4 ... 2.5)	+10% (5% ... 12%)
HiFLOR variable forcing experiment (1971-2015), extrapolated to 1900-2015		1900-2015	2.4× (1.3 ... 8)	+22% (6% ... 41%)

682

683

684

685

686

687

688

689

690

691

692

The sensitivity of precipitation extremes from both models is consistent with that estimated from the gridded observations. The lower-resolution FLOR-FA model shows lower trends than the HiFLOR model. For the HiFLOR model the sensitivity estimated from the SST-restored experiment for 1971–2015 is larger than that from the coupled simulations. Taking into account all modeling results, the probability of an event like south Louisiana 2015 has increased at least by a factor 1.4 due to radiative forcing; the two HiFLOR experiments and the analysis of the full dataset from FLOR-FA suggest central values close to a doubling of probability. Such an increase may be translated to what was once a 1/100 year event somewhere in the Central U.S. Gulf Coast, should now be expected to occur on average, at least once every 70 years, likely even more common. This trend is expected to continue over the 21st century as past and projected future greenhouse forcing continues to warm the planet.

693

694

695

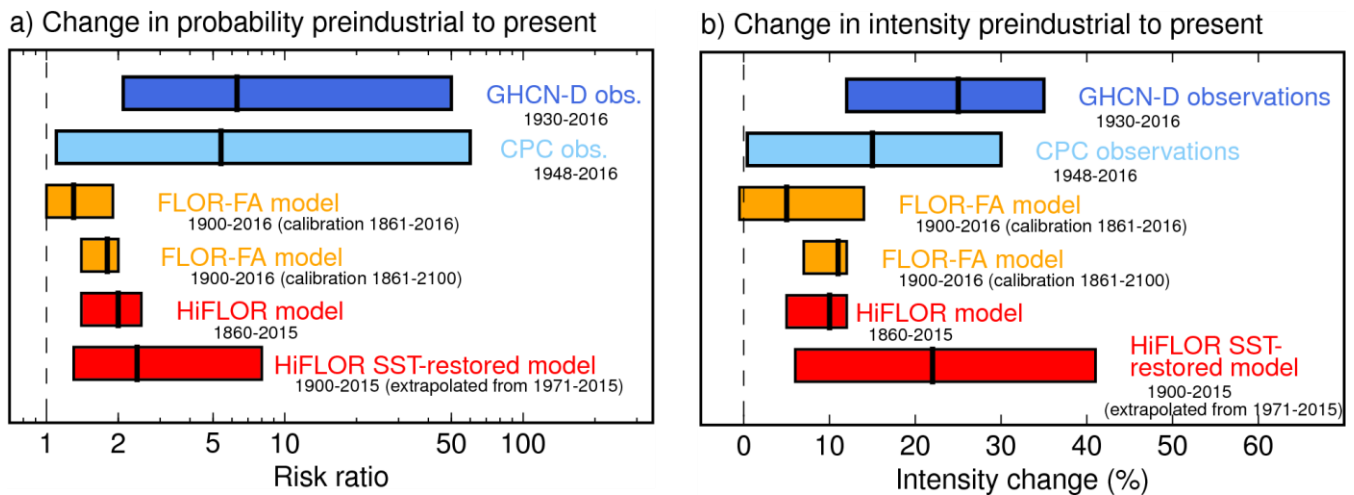
696

697

698

699

The evidence for an influence of the strong 2015/2016 El Niño increasing the probability of the 2016 event is equivocal. The full station dataset shows a statistically significant but small increase in probability, but we do not find the same for the spatial maximum, which represents the strongest events. The FLOR-FA model similarly does not have an ENSO effect, whereas the HiFLOR model again shows a higher probability after a large El Niño. We have found some evidence for decadal Atlantic variability affecting precipitation in the observations, which would have decreased the likelihood in 2016 if confirmed.



700

701 **Figure 15:** Summary of observed (GHCN-D, CPC, blue colors) and modeled (FLOR-FA, HiFLOR, yellow, red
 702 changes in regional precipitation extremes in Central U.S. Gulf Coast. Ranges written in black are the
 703 time periods for which the change is shown over. Calibration for the calculations is done over separate time
 704 periods for noted models. See Table 3 for specific numeric values.

705 7 Discussion

706 We have presented a rapid attribution to climate change and climate variability of the south Louisiana intense
 707 precipitation event. Here we lay out the crucial assumptions made to conduct our assessment, further lines of
 708 inquiry to investigate the validity of the crucial assumptions and the sensitivity of our results to changes in these
 709 assumptions, suggestions for further study on related topics not investigated here, and questions that arise from
 710 this work. Finally, we note some societal impacts ~~and management implications~~ of the findings.

711 7.1 Crucial assumptions

712 In performing these analyses, we have made the following crucial assumptions about ~~the observations, models,~~
 713 the statistical distribution of precipitation extremes, ~~the observations ,and~~ the relationship between temperature
 714 and precipitation extremes, ~~and the models~~. We have tested the sensitivity of our results to some of these
 715 assumptions in the results sections (Sections 3-5) and discuss them below.

- 716 1) We assume that the local, annual maxima of 3-day averaged precipitation over the region of analysis
 717 (29–31 °N, 85–95 °W) can be grouped together, and that their statistical distribution follows a GEV
 718 distribution. Underlying this assumption is that the region has homogeneous extreme precipitation
 719 characteristics (Figure 1f). Furthermore, we assume that all the annual maxima of 3-day averaged
 720 precipitation are drawn from the same statistical distribution, in spite of the many different mechanisms
 721 that lead to extreme precipitation in this region, and that this distribution can be represented well by a
 722 GEV distribution. We further assume that the spatial maximum over the region can also be described
 723 by a GEV.
- 724 2) We assume that analyzing all seasons together provides a fuller distribution of the population of
 725 extreme precipitation events than isolating the analysis to seasons proximate to August (the month in
 726 which the south Louisiana event occurred). In part, the choice to analyse annual extreme events was
 727 motivated by the fact that a variety of meteorological phenomena can lead to extreme precipitation in

728 this region, flooding can occur in any season, and precipitation extremes may change in various
729 seasons (Lehmann et al. 2015, Van der Wiel et al. 2016). All extreme value analyses were repeated
730 focusing only on the JAS season and the qualitative nature of the results was the same as those
731 presented.

732 3) We assume that the inhomogeneities in point station data due to station changes, incomplete records
733 and geographic coverage are smaller than the trends and have no coherent sign. We have checked this
734 by performing the analysis on all stations and for a subset of stations with long (at least 80 year)
735 records and sufficient (0.5°) spatial separation.

736 4) We assume that the methods that create the gridded observationally-based precipitation data result in
737 an accurate representation of 3-day average precipitation at the grid scale. The decorrelation scale of 3-
738 day precipitation is about twice the grid scale, so the largest uncertainty is the inhomogeneous
739 distribution of the gauge stations in space and time. A comparison of the results with point station data
740 shows that the differences are not large.

741 5) We assume that, for the assessment of trends in GEV statistics, global mean surface temperature
742 represents a relevant covariate to capture the *a priori* expected connection between precipitation
743 extremes and temperature (e.g., O’Gorman 2015). A physical motivation for this expected connection
744 is the dependence of the saturation specific humidity of air on temperature through Clausius-Clapeyron
745 (see Section 1). The underlying assumption is that multi-decadal temperature changes exhibit “pattern
746 scaling”, such that global mean temperature change is a sufficient parameter to describe the long-term
747 changes of temperature; furthermore, global-mean temperature helps increase the signal-to-noise ratio
748 of fits to temperature changes. If there is substantial spatial heterogeneity to temperature changes on
749 multi-decadal timescales, the assumption that global mean temperature is the relevant metric becomes
750 suboptimal. Furthermore, if dynamical changes (e.g., changes in the statistics of storms, changes in the
751 dominant moisture sources for extremes, etc.) dominate the observed multi-decadal precipitation
752 extreme changes, this assumption will also be suboptimal.

753 6) We assume that the probability density function of precipitation extremes scales with a covariate, for
754 example (smoothed) global mean temperature and does not exhibit other changes in shape. This
755 assumption is supported by large-sample statistics from modelling experiments such as
756 Weather@Home (Massey et al. 2015) in other regions, but it is not *a priori* obvious that these results
757 should also hold for the Central U.S. Gulf Coast with its wide variety of weather phenomena causing
758 extreme precipitation. Furthermore, the Massey et al. (2015) results were from models of resolution too
759 low to resolve many of the meteorological phenomena that lead to extreme precipitation (e.g. tropical
760 cyclones) in this region.

761 7) We assume that, beyond an initial rapid (~20 year) adjustment to different static radiative forcings, the
762 statistics of precipitation extremes in the static forcing model experiments depend on global mean
763 temperature in the same way as the changes arising from slow drift due to top of the atmosphere
764 radiative disequilibria and slow ocean adjustment. The latter changes are smaller than the forced trend,
765 so the impact of slow model drift on the results is small.

766 8) We assume that the CMIP5 historical forcings (1860-2005) and RCP4.5 forcings (2005-2100), as
767 implemented in the models, are sufficiently accurate representations of the actual changes in radiative

768 forcing that occurred in the real climate system to allow meaningful comparison of modeled changes in
769 precipitation extremes to those observed.

770 9) We assume that the FLOR-FA and HiFLOR modeled responses to changes in radiative forcing are
771 meaningful estimates of the sensitivity of precipitation extremes in the real climate system, since these
772 models capture multiple physical factors affecting precipitation extremes in a physically-based and
773 internally-consistent framework. This assumption is motivated in part because of the ability of these
774 models to simulate large-scale precipitation and temperature over land (e.g., Van der Wiel et al. 2016;
775 Delworth et al. 2015; Jia et al. 2015, 2016), precipitation extremes over the U.S. (Van der Wiel et al.
776 2016), modes of climate variability (e.g., Vecchi et al. 2014; Murakami et al. 2015); the meteorological
777 phenomena that lead to precipitation extremes and their relationship to modes of climate variability
778 (e.g., Vecchi et al. 2014; Krishnamurthy et al. 2015; Murakami et al. 2015, 2016; Zhang et al. 2015,
779 2016; Pascale et al. 2016); and that these models show skill at seasonal predictions of large-scale
780 climate, regional hydrometeorology and the statistics of weather extremes across a broad range of
781 climatic regimes (e.g., Vecchi et al. 2014; Jia et al. 2015, 2016; Yang et al. 2015; Msadek et al. 2015;
782 Murakami et al. 2015, 2016). However, it is important to note that climate models can show a range of
783 global and regional climate sensitivities to changing radiative forcing (e.g., Kirtman et al. 2013, Collins
784 et al. 2013)

785

786 These assumptions were crucial to enable a rapid assessment of the climate context of the extreme
787 precipitation of the August 2016 south Louisiana event. Subsequent analyses should further assess the validity
788 of these assumptions, and the quantitative impact of failures in their validity. Below we outline our present
789 evaluation of the implications of these choices and potential areas of further research.

790 Sensitivity experiments should be produced by varying the parameters of our study. We did not
791 conduct analysis of how the size of our defined box for the Central U.S. Gulf Coast affects our results (crucial
792 assumption 1). If the region is altered to remove points that have greater risks relative to those included, the
793 findings may change. Changes in extreme precipitation risks in the Central U.S. Gulf Coast should not be
794 applied elsewhere without further investigation. Temporally, we were able to validate the seasonal distribution
795 of precipitation extremes in models and observations (Section 4.1), and redid the analysis for JAS only, which
796 gave larger uncertainties and somewhat smaller trends (crucial assumption 2). Future work could further
797 quantify seasonal differences in extremes and their response to climate forcing. Similarly, to sample the spread
798 in sensitivity to future RCP forcings (crucial assumption 8, used for any modeled years beyond 2005), our
799 results may be revised with different climate forcings. For the near term however, this is likely not an issue in
800 HiFLOR (used to produce climates for 2005-2015 in the static forcing and nudged SST runs) as climate
801 variability tends to be greater than the climate response to different scenarios during this time period (Forster et
802 al. 2013; Hawkins and Sutton 2009; Kirtman and Power 2013), but may affect future climate results in the
803 FLOR-FA variable forcing experiment at the end of the century (2100, Hawkins and Sutton 2009).
804 FinallyFurthermore, the appropriateness of GEV fits in general should be tested (crucial assumptions 1,6).

805 Sensitivity experiments of our results to model bias and integration length (or length of the observed
806 record) should be produced (crucial assumptions 3 and 7). Short records limit the reliability of the statistics of
807 precipitation extremes. This is important for our model validation of the annual cycle of extremes (Section 4.1)

808 and for the comparison of modeled and observed GEV fits (Section 5). The statistics of precipitation extremes in
809 HiFLOR are closer to those observed than the statistics in FLOR-FA. However, we note that the model
810 experiments with FLOR-FA are significantly longer and therefore provide better statistics of its (biased) climate
811 than the experiments with HiFLOR or the observed record. It cannot thus be fully-excluded that the double
812 distribution of extremes in FLOR-FA or the large peak in JAS in extreme precipitation intensity is purely a
813 result of model bias.

814 A portion of the beginning of the static forcing experiments have been disregarded to allow the model
815 to spin-up in response to radiative forcing. GEV fits were originally calculated by disregarding the first 10 years
816 of data to allow for spin-up, but was extended to 20 years to provide the simulated climate more time to
817 approach equilibrium (crucial assumption 7). The results are only altered slightly by this sensitivity test. Given
818 the length of the available ensemble suite of static forcing experiments, disregarding more years in the
819 beginning of the simulation would reduce our ability to sample extremes. With longer integrations of static
820 forcing experiments and additional ensemble members, we would have more information to assess how model
821 spin-up may affect our results. Similarly, longer integrations would allow for an assessment of the impact of
822 model drift due to ocean adjustment (crucial assumption 7).

823 The attribution to climate change presented here depends on our assumption that changes in
824 precipitation extremes scale with global mean temperature and do not arise from changes in the shape of their
825 underlying distribution (crucial assumptions 5 and 6). The thermodynamic basis of this assumption is based on a
826 large body of research (O’Gorman 2015), however as noted before there is a large variety of synoptic systems
827 that may cause precipitation extremes in the Gulf Coast region. It is not obvious that possible impacts of
828 changes in synoptic weather patterns scale with global mean temperatures. For example, the frequency, track
829 location and/or intensity of tropical cyclones (responsible for 7 out of the 9 most extreme events in JAS were
830 related to tropical cyclones, Figure 8) can each change in complex ways that need not scale with each other or
831 global mean temperature (e.g., Vecchi and Soden 2007; Murakami and Wang 2010; Emanuel and Sobel 2013;
832 Emanuel et al. 2013; Knutson et al. 2013; Vecchi et al. 2013; Walsh et al. 2015), and could cause changes to the
833 statistics of extreme rainfall in the Central U.S. Gulf Coast. Further research must investigate what the impact of
834 dynamic changes (e.g. frequency of occurrence of various synoptic systems, dominant moisture sources,
835 precipitation efficiency) is on the presented trend of precipitation extremes.

836 To investigate the sensitivity of the results to the chosen observational data sets (both based on rain
837 gauge measurements, crucial assumption 3 and 4), we suggest repeating the current analysis with an
838 independent observational estimate of current and historical precipitation along the Gulf coast (e.g. estimates
839 based on satellite data). Furthermore, though we use two global climate models (FLOR-FA and HiFLOR,
840 crucial assumptions 7 and 9) and various experimental setups (static radiative forcing, time-varying radiative
841 forcing and restoring observed SST variability), the models are part of the same NOAA/GFDL family.
842 Consequently, they exhibit similar patterns of (surface temperature) bias and rely on the same parameterization
843 schemes for precipitation. Further inquiry for understanding model-specific biases that may impact the results
844 may still be warranted. For example, there is a North Atlantic cold bias in the models, thought to be connected
845 in part to inadequate eddy parameterizations and a resulting cloud feedback (Delworth et al. 2006; Delworth et
846 al. 2012; Vecchi et al. 2014; Murakami et al. 2015). This may be the source of higher magnitudes of modeled
847 extreme precipitation found due to climate variability in the HiFLOR restored-SST experiments. An assessment

848 using different climate models would therefore add value to allow for a sampling of risk across models, in
849 addition to across experimental setups. These will be available shortly in the HighResMIP project (Haarsma et
850 al. 2016).

851 **7.2 Future work and broader impacts**

852 As described in the introduction and methods, we have purposefully focused our present assessment on
853 one aspect of the flooding problem: the risk of extreme precipitation events that have the potential to produce
854 inland flooding. We have provided provisional streamgauge data in the introduction (Figure 2) to illustrate the
855 effect of the August 2016 event, but have not examined flood risks in the region from streamgauge data directly.
856 Part of the reason for this is that real-time streamgauge data is provisional and subject to revision, which can be
857 exacerbated during a flood when gauges can be overtopped and have missing data due to high water volumes or
858 streamgauge malfunctions (Rantz 1982). The USGS advises users to cautiously consider the use of provisional
859 streamgauge data for decision making (official USGS provisional policy available:
860 <<https://water.usgs.gov/wateralert/provisional/>>). A complimentary modeling study of land surface conditions
861 and interactions with the river environment also requires a more local modeling approach, potentially with a
862 hydrologic model with information on the river system and small scale water processes, and conceivably
863 including an estimate of the impact of direct human impacts (through urbanization, water diversion and
864 management, etc.) which under our time constraints, data access, and present capabilities of our climate models
865 was not feasible.

866 It is important to distinguish extreme precipitation events that are the topic of this study, motivated by
867 the August 2016 rain event that led to devastating “freshwater” or “inland” flooding in south Louisiana, from
868 events that lead to “coastal” or “saltwater” flooding. In particular, the climate change context of saltwater
869 flooding must include an assessment of the regional sea level change contributions and meteorological
870 conditions that can influence these types of events (e.g., Katsman et al, 2008, Sterl et al, 2012, Lin et al. 2012,
871 2014, Little et al. 2014). While certain meteorological conditions, such as landfalling tropical cyclones, can lead
872 to both freshwater and saltwater flooding (e.g., Lin et al. 2012, Villarini et al. 2014), the assessments and
873 discussions presented here are only relevant to extreme rainfall events that have the potential to initiate inland
874 flooding; we do not address changes in storm surges, nuisance flooding (Moftakhari et al. 2015) or other
875 saltwater flooding events.

876 Dependence of the statistics of extreme precipitation events in the Central U.S. Gulf Coast on large-scale
877 climate drivers could provide a scientific basis for seasonal predictions of the odds of these events, much as is
878 now regularly done for the statistics of hurricanes. However, as we show in Section 3.3, we are unable to find
879 strong connections between the statistics of these extreme precipitation events and modes of SST variability
880 (e.g., ENSO), which suggests the possibility for limited seasonal predictability for these events beyond the
881 multi-decadal increase in probability from long-term climate warming. However, potential sources of
882 predictability may be uncovered by future refined analyses.

883 The extent to which the changing risk of extreme rainfall events like that in south Louisiana has
884 implications for stakeholders, such as homeowners, local and federal governments, the humanitarian system,
885 and the insurance industry, will depend on details of the exposure, vulnerability and the disaster preparedness
886 and response strategies available to each. Changes to the physical system are a key factor in adaptation and

887 decisions, but these factors operate in a complex landscape. Through a disaster management lens, the increased
888 frequency of this type of event found in this study may place strains on humanitarian responders and
889 institutions, ~~especially in the future if this type of extreme event continues to become more frequent now and in~~
890 ~~the future~~. Knowing the change in return periods of the most extreme events can help to provide insight into
891 how humanitarian institutions can evolve to be prepared for the future; in addition to adapting to a broader trend
892 of increasing hydro-meteorological disasters globally (CRED 2015). A worthwhile topic to explore in further
893 assessment of this and related events is the extent to which public and media perception both before (local
894 preparedness, willingness to evacuate) and after (nationwide media coverage and awareness of impacts) may
895 have been impacted by the fact that the storm was not named. However, there is an insufficiency of peer-
896 reviewed literature on this topic, even as media outlets in the UK and U.S. have started naming winter storms
897 following the German example (Cutlip 2013, Van Oldenborgh et al. 2015).

898 It is essential to note that this analysis has pursued an assessment of the climate change context of
899 extreme precipitation events (a “climate attribution” study) in which we evaluate the impact of climate
900 conditions and changes in radiative forcing on the probability of extreme rainfall events in south Louisiana and
901 the Central U.S. Gulf Coast. This analysis is fundamentally different in nature from (and complementary to)
902 assessments of the synoptic chain of events that led to the particular Louisiana extreme precipitation event in
903 August 2016 (we would label that “synoptic attribution”). Synoptic attribution of the event generally involves a
904 clear chain of events that led to the extreme rainfall event in a relatively deterministic fashion. Meanwhile, the
905 climate attribution presented here is fundamentally probabilistic. Although we recognize that the synoptic
906 context of this particular extreme event is unique (in fact all events are unique in detail), we have sought to
907 understand the climate context of the probabilities of a class of events that causes extreme precipitation in the
908 Central U.S. Gulf Coast of which this event (flood-inducing extreme precipitation in south Louisiana) is a
909 member (Otto et al, 2016). Furthermore, it is possible to assess the climatic context in more detail, by assessing
910 more proximate climate drivers than global-mean temperature or radiative forcing (e.g., by looking at the impact
911 of particular patterns of SST), or by a more refined assessment of the detailed impact of the superposition of
912 modes of climate variability and multi-decadal climate change (e.g., Delworth et al. 2015, Jia et al. 2016). For
913 any particular event a spectrum of attribution studies (from purely synoptic to purely climate) could, and
914 perhaps should, be pursued in order to unravel the various factors relevant to that event. Moreover, some of
915 these studies are feasible at rapid attribution timescales while others require more time and focused resources to
916 produce the specific and targeted modeling experiments and observational analyses.

917 ~~Our ability to perform the climate attribution of this event was made possible by~~ Climate attribution
918 studies such as this one can only be performed with pre-existing multi-centennial global simulations with high
919 spatial resolution models, ~~which~~ This allowed us to efficiently assess the impact of radiative forcing changes
920 on regional extreme precipitation events. These simulations, obviously, necessitated the long-term research
921 aimed at developing these high-resolution models (e.g., Putnam and Lin 2007, Delworth et al. 2012, Vecchi et
922 al. 2014, Murakami et al. 2015). Furthermore, this work was enabled by a body of work using these models that
923 provided the necessary understanding of the characteristics and fidelity of these models to simulate large-scale
924 and regional climate, and weather events over a broad range of scales and phenomena (e.g., Vecchi et al. 2014;
925 Msadek et al. 2014; Delworth et al. 2015; Jia et al. 2015, 2016; Murakami et al. 2015, 2016; Krishnamurthy et
926 al. 2015; Zhang et al. 2015, 2016; Pascale et al. 2016; Van der Wiel et al. 2016).

927 In particular, this paper follows on a recent analysis of the climatology and CO₂ sensitivity of extreme
928 precipitation events over the U.S. in these same models, showing that FLOR and HiFLOR in particular are
929 uniquely capable of capturing Central U.S. Gulf Coast precipitation extremes, which has large biases in coarser
930 resolution models (Van der Wiel et al. 2016). Though the analysis of extreme precipitation events in Van der
931 Wiel et al. (2016) is of a different nature (focusing on much lower return period events, using different statistical
932 methods, and focusing at the grid point scale rather than regional events), the results presented there are
933 consistent with the current analysis. The previous paper showed that in response to increasing CO₂ levels in the
934 atmosphere, precipitation extremes along the Central U.S. Gulf Coast increase in intensity, with less likely
935 events exhibiting larger fractional intensity increases.

936 We have here sought to provide a scientifically rigorous rapid assessment of the climate context of this
937 precipitation event, which had tragic consequences, to provide meaningful grounding to the public discussions
938 of this event, given both the intense interest in this specific event and our ongoing work on the general subject of
939 climate and extremes (and precipitation extremes in the U.S. in particular, Van der Wiel et al. 2016). We hope
940 that this study, including our explicit discussion of the assumptions needed to pursue this accelerated
941 assessment, will help push the scientific conversation forward to improve our understanding of the risks and
942 return periods of extreme precipitation in the Central U.S. Gulf Coast. The field of rapid attribution analysis is
943 still nascent and may one day lead to such assessments being the normal course of action in response to an
944 extreme event to help provide scientific basis for real-time discussions, and in longer-term disaster response and
945 rebuilding. Until that time, studies such as this will likely only be done for select regions and event types where
946 there is sufficient easily accessible data, and a team of scientists with the necessary expertise and ability to make
947 time in their schedules to provide a rapid assessment. We expect that these early efforts at event attribution will
948 expand our knowledge and capabilities on this subject, and facilitate further inquiry.

949 **Acknowledgements**

950 We thank Geert Lenderink, Sarah Kew, Nathaniel Johnson, Kieran Bhatia and Fanrong Zeng for their helpful
951 comments on an earlier version of the manuscript. Funding for this work was supplied by the National Oceanic
952 and Atmospheric Administration, U.S. Department of Commerce to the Geophysical Fluid Dynamics
953 Laboratory, to the Cooperative Institute for Climate Science (award NA14OAR4320106). The statements,
954 findings, conclusions, and recommendations are those of the authors and do not necessarily reflect the views of
955 the National Oceanic and Atmospheric Administration, or the U.S. Department of Commerce, or other affiliated
956 institutions. This project was made possible through generous support from donors to Climate Central's World
957 Weather Attribution initiative and the EU project EUCLEIA under Grant Agreement 607085. CPC U.S. Unified
958 Precipitation data provided by the NOAA/OAR/ESRL PSD, Boulder, Colorado, U.S. and can be downloaded
959 from: from <http://www.esrl.noaa.gov/psd/>. USGS data was obtained from the automated website and are
960 provisional and subject to revision. The data are released on the condition that neither the USGS nor the United
961 States Government may be held liable for any damages resulting from its use.

962 **Data availability**

963 NOAA GFDL climate model data is not readily available globally at all grid points and for all simulations
964 owing to the size of daily global climate model output for high resolution models with thousands of years of

965 simulations (on the order of 100x terabytes). We have made the precipitation data for the Central U.S. Gulf
966 Coast, global temperature and ENSO data that were used in this study available at the Climate Explorer:
967 <http://climexp.knmi.nl/selectfield_att.cgi>.

968 **References**

- 969 Allen, R. and Burgess, R.: LSU AgCenter predicts floods cost state at least \$110 million in crop loss. The
970 Advocate, viewed 26 August 2016. <[http://www.theadvocate.com/louisiana_flood_2016/article_a7689806-
971 6946-11e6-a681-ab59c458f55c.html?sr_source=lift_amplify](http://www.theadvocate.com/louisiana_flood_2016/article_a7689806-6946-11e6-a681-ab59c458f55c.html?sr_source=lift_amplify)>
- 972 American Red Cross: Louisiana Flooding: Red Cross Shelters 10,000+ After Worst Disaster Since Superstorm
973 Sandy. *American Red Cross*, viewed August 23 2016, [http://www.redcross.org/news/press-release/Louisiana-
974 Flooding-Red-Cross-Shelters-10000-After-Worst-Disaster-Since-Superstorm-Sandy](http://www.redcross.org/news/press-release/Louisiana-Flooding-Red-Cross-Shelters-10000-After-Worst-Disaster-Since-Superstorm-Sandy)
- 975 American Red Cross: Needs of People in Louisiana Remain Great; Red Cross Still Sheltering 7,000+, Serving
976 Thousands of Meals. *American Red Cross*, viewed 23 August 2016, <[http://www.redcross.org/news/press-
977 release/Needs-of-People-in-Louisiana-Remain-Great-Red-Cross-Still-Sheltering-7000-Serving-Thousands-of-
978 Meals](http://www.redcross.org/news/press-release/Needs-of-People-in-Louisiana-Remain-Great-Red-Cross-Still-Sheltering-7000-Serving-Thousands-of-Meals)>.
- 979 Broach, D.: How many houses, people flooded in Louisiana? *NOLA*, viewed 24 August 2016,
980 <http://www.nola.com/weather/index.ssf/2016/08/how_many_people_houses_were_fl.html>.
- 981 Bromwich, J.E.: Flooding in the South Looks a Lot Like Climate Change, *The New York Times*, viewed 24
982 August 2016, <<http://www.nytimes.com/2016/08/17/us/climate-change-louisiana.html>>.
- 983 Burton, J. and A. Demas: Six streamgages Set peaks of record and 50 stations were overtopped by floodwaters.
984 *USGS*, viewed 22 August 2016, <<https://www.usgs.gov/news/usgs-records-historic-flooding-south-louisiana>>.
- 985 Centre for Research on the Epidemiology of Disasters (CRED): The Human Cost of Natural Disasters 2015, A
986 Global Perspective; ReliefWeb, viewed on 29 August 2016
987 http://reliefweb.int/sites/reliefweb.int/files/resources/PAND_report.pdf
- 988 Chen, C.-T., and Knutson, T.: On the verification and comparison of extreme rainfall indices from climate
989 models. *J. Climate*, 21 (7), 1605–1621, 2008.
- 990 Christidis, N., Stott, P.A., Scaife, A.A., Arribas, A., Jones, G.S., Copesey, D., Knight, J.R. and Tennant, W.J.: A
991 new HadGEM3-A-based system for attribution of weather-and climate-related extreme events. *J. Climate*,
992 26(9), pp.2756-2783, 2013.
- 993 Collins, M., Knutti, R., Arblaster, J., Dufresne, J.-L., Fichefet, T., Friedlingstein, P., Gao, X., Gutowski, W.J.,
994 Johns, T., Krinner, G., Shongwe, M., Tebaldi, C., Weaver, A.J., and Wehner, M.: Long-term Climate Change:
995 Projections, Commitments and Irreversibility. In *Climate Change 2013: The Physical Science Basis, Contribution of Working Group I to the Fifth Assessment Report of the Intergovernmental Panel on Climate Change*. [Stocker, T.F., Qin, D., Plattner, G.-K., Tignor, M., Allen, S.K., Boschung, J., Nauels, A., Xia, Y., Bex, V., and Midgley, P.M. (eds.)]. Cambridge University Press, Cambridge, United Kingdom and New York, NY, USA. 2013.
- 1000 Coles, S.: *An Introduction to Statistical Modeling of Extreme Values*, Springer Series in Statistics, London, UK,
1001 2001.
- 1002 Cutlip, K 2013, 'Weather Front', *Weatherwise*, 66, 2, p. 6, MAS Ultra - School Edition, EBSCOhost, viewed 29
1003 August 2016.
- 1004 Dai, A.: Precipitation characteristics in eighteen coupled climate models. *J. Climate*, 19(18), 4605-4630, 2006.
- 1005 Davies, R.: Louisiana Rivers at Record Levels, President Declares Major Disaster. *Floodlist*, viewed 23 August
1006 2016, <<http://floodlist.com/america/usa/usa-louisiana-rivers-record-levels-president-declares-major-disaster>>.
- 1007 Delworth, T.L., Broccoli, A.J., Rosati, A., Stouffer, R.J., Balaji, V., Beesley, J.A., Cooke, W.F., Dixon, K.W.,
1008 Dunne, J., Dunne, K.A. and Durachta, J.W., Findell, K., Ginoux, P., Gnanadesikan, A., Gordon, C.T., Griffies, S.,
1009 Gudgel, R., Harrison, M., Held, I., Hemler, R., Horowitz, L., Klein, S., Knutson, T., Kushner, P.,
1010 Langenhorst, A., Lee, H.-C., Lin, S.-J., Lu, J., Malyshev, S., Milly, P.C.D., Ramaswamy, V., Russell, J.,
1011 Schwarzkopf, M.D., Shevliakova, E., Sirutis, j., Spelman, M., Stern, W., Winton, M., Wittenberg, A., Wyman,

1012 B., Zeng, F., Zhang, R.: GFDL's CM2 global coupled climate models. Part I: Formulation and simulation
1013 characteristics. *J. Climate*, 19(5), 643-674, 2006.

1014 Delworth, T.L., Rosati, A., Anderson, W., Adcroft, A.J., Balaji, V., Benson, R., Dixon, K., Griffies, S.M., Lee,
1015 H.C., Pacanowski, R.C., Vecchi, G.A., Wittenberg, A.T., Zeng, F., and Zhang, R.: Simulated climate and
1016 climate change in the GFDL CM2. 5 high-resolution coupled climate model. *J. Climate*, 25(8), 2755-2781,
1017 2012.

1018 Delworth, T.L., Zeng, F., Rosati, A., Vecchi, G.A. and Wittenberg, A.T.: A link between the hiatus in global
1019 warming and North American drought. *J. Climate*, 28(9), 3834-3845, 2015.

1020 [Efron, B. and Tibshirani, R. J., 1998. *An introduction to the bootstrap*, Chapman and Hall, New York. 439pp.](#)

1021 Eggert, B., Berg, P., Haerter, J.O., Jacob, D. and Moseley, C.: Temporal and spatial scaling impacts on extreme
1022 precipitation. *Atmospheric Chemistry and Physics*, 15(10), 5957-5971, 2015.

1023 Emanuel, K., and Sobel, A.: Response of tropical sea surface temperature, precipitation, and tropical cyclone-
1024 related variables to changes in global and local forcing. *J. of Advances in Modeling Earth Systems*,
1025 doi:10.1002/jame.20032, 2013.

1026 Emanuel, K., Solomon, S., Folini, D., Davis, S., and Cagnano, C.: Influence of Tropical Tropopause Layer
1027 Cooling on Atlantic Hurricane Activity. *J. Climate*, doi:10.1175/JCLI-D-12-00242.1, 2013

1028 FEMA: Federal Support for Louisiana Continues, \$127 Million in Financial Assistance Provided to Louisiana
1029 Flood Survivors So Far. FEMA, viewed 23 August 2016, <[https://www.fema.gov/news-
1030 release/2016/08/23/federal-support-louisiana-continues-127-million-financial-assistance](https://www.fema.gov/news-release/2016/08/23/federal-support-louisiana-continues-127-million-financial-assistance)>

1031 Flato, G., Marotzke, J., Abiodun, B., Braconnot, P., Chou, S.C., Collins, W.J., Cox, P., Driouech, F.,
1032 Emori, S., Eyring, V. and Forest, C., Gleckler, P., Guilyardi, E., Jakob, C., Kattsov, V., Reason, C.,
1033 Rummukainen, M.: *Evaluation of Climate Models. In: Climate Change 2013: The Physical Science Basis.*
1034 *Contribution of Working Group I to the Fifth Assessment Report of the Intergovernmental Panel on*
1035 *Climate Change*. Climate Change 2013, 5,741-866, 2013.

1036 Forster, P. M., T. Andrews, P. Good, J. M. Gregory, L. S. Jackson, and M. Zelinka: Evaluating adjusted
1037 forcing and model spread for historical and future scenarios in the CMIP5 generation of climate models, *J.*
1038 *Geophys. Res. Atmos.*, 118, 1139–1150, doi:10.1002/jgrd.50174, 2013.

1039 Gandin, L. S., and R. Hardin: *Objective analysis of meteorological fields*, Vol. 242. Israel program for scientific
1040 translations Jerusalem, 1965.

1041 GISTEMP Team: GISS Surface Temperature Analysis (GISTEMP). NASA Goddard Institute for Space Studies.
1042 Dataset accessed 2016-08-08 at <<http://data.giss.nasa.gov/gistemp/>>.

1043 Haarsma, R. J., Roberts, M., Vidale, P. L., Senior, C. A., Bellucci, A., Bao, Q., Chang, P., Corti, S.,
1044 Fučkar, N. S., Guemas, V., von Hardenberg, J., Hazeleger, W., Kodama, C., Koenigk, T., Leung, L. R.,
1045 Lu, J., Luo, J.-J., Mao, J., Mizielinski, M. S., Mizuta, R., Nobre, P., Satoh, M., Scoccimarro, E., Semmler,
1046 T., Small, J., and von Storch, J.-S.: High Resolution Model Intercomparison Project (HighResMIP),
1047 *Geosci. Model Dev. Discuss.*, doi:10.5194/gmd-2016-66, in review, 2016.

1048 Hansen, J., Ruedy, R., Sato, M. and Lo, K.: Global surface temperature change. *Reviews of Geophysics*, 48(4),
1049 2010.

1050 Harris, L.M, Lin, S.-J., and Tu, C.Y.: High resolution climate simulations using GFDL HiRAM with a stretched
1051 global grid. *J. Climate*, 29, 4293–4314, 2016.

1052 Hawkins, E. and Sutton, R.: The potential to narrow uncertainty in regional climate predictions. *Bulletin of the*
1053 *American Meteorological Society*, 90(8), 1095, 2009.

1054 Hazeleger, W. Wang, X., Severijns, C., Stefanescu, S., Bintanja, R., Sterl, A., Wyser, K., Semmler, T, Yang, S.,
1055 Van den Hurk, B., Van Noije, T., Van der Linden, E., Van der Wiel, K.: EC-Earth V2.2: description and
1056 validation of a new seamless earth system prediction model. *Clim.Dyn.*, 39, 2611-2629, 2012.

1057 Hazeleger, W., Wouters, B., Oldenborgh, G.J., Corti, S., Palmer, T., Smith, D., Dunstone, N., Kröger, J.,
1058 Pohlmann, H. and Storch, J.S.: Predicting multiyear north atlantic ocean variability. *Journal of Geophysical*
1059 *Research: Oceans*, 118(3), 1087-1098, 2013.

1060 Herscher, R.: “Flooding in Louisiana Raises Questions About Timing, Urgency of Warnings” *NPR*, viewed 29
1061 August 2016, <<http://www.npr.org/sections/thetwo-way/2016/08/22/490916070/flooding-in-louisiana-raises-questions-about-timing-urgency-of-warnings>>.

1063 Higgins, R. W., W. Shi, E. Yarosh, and R. Joyce: Improved United States precipitation quality control system
1064 and analysis. NOAA, National Weather Service, National Centers for Environmental Prediction, *Climate*
1065 *Prediction Center Atlas*, 2000.

1066 Huang, B., Banzon, V.F., Freeman, E., Lawrimore, J., Liu, W., Peterson, T.C., Smith, T.M., Thorne, P.W.,
1067 Woodruff, S.D. and Zhang, H.M.: Extended reconstructed sea surface temperature version 4 (ERSST. v4). Part
1068 I: upgrades and intercomparisons. *J. Climate*, 28(3), 911-930, 2015.

1069 Jia, L., Yang, X., Vecchi, G.A., Gudgel, R.G., Delworth, T.L., Rosati, A., Stern, W.F., Wittenberg, A.T.,
1070 Krishnamurthy, L., Zhang, S. and Msadek, R.: Improved seasonal prediction of temperature and precipitation
1071 over land in a high-resolution GFDL climate model. *J. Climate*, 28(5), 2044-2062, 2015.

1072 Jia, L., Vecchi, G.A., Yang, X., Gudgel, R., Delworth, T., Stern, W., Paffendorf, K., Underwood, S., Zeng, F.:
1073 The Roles of Radiative Forcing, Sea Surface Temperatures, and Atmospheric and Land Initial Conditions in
1074 U.S. Summer Warming Episodes. *J. Climate*, doi:10.1175/JCLI-D-15-0471.1, 2016.

1075 Kalnay, E., Kanamitsu, M., Kistler, R., Collins, W., Deaven, D., Gandin, L., Iredell, M., Saha, S., White, G.,
1076 Woollen, J. and Zhu, Y.: The NCEP/NCAR 40-year reanalysis project. *Bulletin of the American meteorological*
1077 *Society*, 77(3), 437-471, 1996.

1078 Katsman, C.A., Hazeleger, W., Drijfhout, S.S., van Oldenborgh, G.J. and Burgers, G.: Climate scenarios of sea
1079 level rise for the northeast Atlantic Ocean: a study including the effects of ocean dynamics and gravity changes
1080 induced by ice melt. *Climatic Change*, 91(3-4), 351-374, 2008.

1081 Keim, B.D. and Faiers, G.E.: Heavy rainfall distributions by season in Louisiana: Synoptic interpretations and
1082 quantile estimates. *Water Resources Bulletin*, 32(1), 117-124, 1996.

1083 Kirtman, B., Power, S.B., Adedoyin, J.A., Boer, G.J., Bojariu, R., Camilloni, I., Doblas-Reyes, F.J., Fiore,
1084 A.M., Kimoto, M., Meehl, G.A., Prather, M., Sarr, A., Schär, C., Sutton, R., Van Oldenborgh, G.J., Vecchi, G.,
1085 and Wang, H.-J.: Near-term climate change: projections and predictability. In *Climate Change 2013: The*
1086 *Physical Science Basis, Contribution of Working Group I to the Fifth Assessment Report of the*
1087 *Intergovernmental Panel on Climate Change*. [Stocker, T.F., Qin, D., Plattner, G.-K., Tignor, M., Allen, S.K.,
1088 Boschung, J., Nauels, A., Xia, Y., Bex, V., and Midgley, P.M. (eds.)]. Cambridge University Press, Cambridge,
1089 United Kingdom and New York, NY, USA. 2013.

1090 Knapp, K.R., Kruk, M.C., Levinson, D.H., Diamond, H.J. and Neumann, C.J.: The international best track
1091 archive for climate stewardship (IBTrACS). *Bulletin of the American Meteorological Society*, 91(3), 363, 2010.

1092 Knutson, T.R., Sirutis, J.J., Vecchi, G.A., Garner, S., Zhao, M., Kim, H.S., Bender, M., Tuleya, R.E., Held, I.M.
1093 and Villarini, G.: Dynamical downscaling projections of twenty-first-century Atlantic hurricane activity: CMIP3
1094 and CMIP5 model-based scenarios. *J. Climate*, 26(17), 6591-6617, 2013.

1095 Krishnamurthy, L., Vecchi, G., Msadek, R., Wittenberg, A., Delworth, T., and Zeng, F.: The Seasonality of the
1096 Great Plains Low-Level Jet and ENSO Relationship. *J. Climate*. doi:10.1175/JCLI-D-14-00590.1, 2015.

1097 Lehmann, J., Coumou, D. and Frieler, K.: Increased record breaking precipitation events under global
1098 warming. *Climatic Change*, 132(4), 501-505, doi:10.1007/s10584-015-1434-y, 2015.

1099 Lenderink, G. and Attema, J.: A simple scaling approach to produce climate scenarios of local precipitation
1100 extremes for the Netherlands. *Environmental Research Letters*, 10(8), 085001, 2015.

1101 Little, C.M., Horton, R.M., Kopp, R.E., Oppenheimer, M., Vecchi, G.A., and Villarini, G.: Joint projections of
1102 US East Coast sea level and storm surge. *Nature Climate Change*. doi:10.1038/nclimate2801, 2015.

1103 Lin, N., Emanuel, K., Oppenheimer, M. and Vanmarcke, E.: Physically based assessment of hurricane surge
1104 threat under climate change. *Nature Climate Change*, 2(6), 462-467, 2012.

1105 Lin, N., Lane, P., Emanuel, K.A., Sullivan, R.M., and Donnelly, J.P.: Heightened hurricane surge risk in
1106 northwest Florida revealed from climatological-hydrodynamic modeling and paleorecord reconstruction. *J.*
1107 *Geophys. Res. (Atmospheres)*, doi:10.1002/2014JD021584, 2014

1108 Massey, N., Jones, R., Otto, F.E.L., Aina, T., Wilson, S., Murphy, J.M., Hassell, D., Yamazaki, Y.H., and M.R.
1109 Allen: weather@home - development and validation of a very large ensemble modelling system for probabilistic
1110 event attribution. *Q. J. Royal Met. Soc.*, doi:10.1002/qj.2455, 2015.

1111 Menne, M.J., I. Durre, R.S. Vose, B.E. Gleason, and T.G. Houston: An overview of the Global Historical
1112 Climatology Network-Daily Database. *Journal of Atmospheric and Oceanic Technology*, 29, 897-910, 2012.
1113

1114 Menne, M.J., I. Durre, B. Korzeniewski, S. McNeal, K. Thomas, X. Yin, S. Anthony, R. Ray, R.S. Vose,
1115 B.E. Gleason, and T.G. Houston: Global Historical Climatology Network-Daily (GHCN-Daily), Version 3.22.
1116 NOAA National Climatic Data Center. <http://doi.org/10.7289/V5D21VHZ> 19 August 2016.

1117 De Michele, C. and Salvadori, G.: On the derived flood frequency distribution: analytical formulation and the
1118 influence of antecedent soil moisture condition. *Journal of Hydrology*, 262(1), 245-258, 2002.

1119 Milman, O.: Disasters like Louisiana floods will worsen as planet warms, scientists warn, *The Guardian*, viewed
1120 24 August 2016, <[https://www.theguardian.com/environment/2016/aug/16/louisiana-flooding-natural-disaster-
1121 weather-climate-change](https://www.theguardian.com/environment/2016/aug/16/louisiana-flooding-natural-disaster-weather-climate-change)>.

1122 Moftakhari, H.R., AghaKouchak, A., Sanders, B.F., Feldman, D.L., Sweet, W., Matthew, R.A. and Luke, A.:
1123 Increased nuisance flooding along the coasts of the United States due to sea level rise: Past and future. *Geophys.*
1124 *Res. Lett.*, 42(22), 2015.

1125 Msadek, R., Vecchi, G.A., Winton, M., Gudgel, R.: Importance of initial conditions in seasonal predictions of
1126 Arctic sea ice extent. *Geophys. Res. Lett.*, DOI: 10.1002/2014GL060799, 2014.

1127 Murakami, H., and Wang, B.: Future Change of North Atlantic Tropical Cyclone Tracks: Projection by a 20-
1128 km-Mesh Global Atmospheric Model. *J. Climate*, doi:10.1175/2010JCLI3338.1, 2010.

1129 Murakami, H., Vecchi, G.A., Underwood, S., Delworth, T., Wittenberg, A.T., Anderson, W., Chen, J.-H.,
1130 Gudgel, R., Harris, L., Lin, S.-J., and Zeng, F.: Simulation and prediction of Category 4 and 5 hurricanes in the
1131 high-resolution GFDL HiFLOR coupled climate model. *J. Climate*, doi:10.1175/JCLI-D-15-0216.1, 2015.

1132 Murakami, H., Vecchi, G.A., Villarini, G., Delworth, T., Gudgel, R., Underwood, S.D., Yang, X., Zhang, W.,
1133 Lin, S.-J.: Seasonal Forecasts of Major Hurricanes and Landfalling Tropical Cyclones using a High-Resolution
1134 GFDL Coupled Climate Model. *J. Climate*, 10.1175/JCLI-D-16-0233.1, 2016.

1135 National Weather Service: Southern and Eastern U.S. Heavy Rainfall, storm summaries 1-19, viewed 23 August
1136 2016, <http://www.wpc.ncep.noaa.gov/winter_storm_summaries/storm15/storm15_archive.shtml> and New
1137 Orleans area forecast discussions (PIL=AFDLIX), viewed 24 August 2016,
1138 <<https://mesonet.agron.iastate.edu/wx/afos/>>.

1139 O’Gorman, P.A.: Precipitation extremes under climate change. *Current climate change reports*, 1(2), 49-59,
1140 2015.

1141 Otto, F.E., Van Oldenborgh, G.J., Eden, J., Stott, P.A., Karoly, D.J. and Allen, M.R.: The attribution question.
1142 *Nature Climate Change*, 6(9), pp.813-816, 2016.

1143 Pascale, S., Bordoni, S., Kapnick, S.B., Vecchi, G.A., Jia, L., Delworth, T.L., Underwood, S. Anderson, W.:
1144 The impact of horizontal resolution on North American monsoon Gulf of California moisture surges in a suite
1145 of coupled global climate models. *J. Climate*, doi:10.1175/JCLI-D-16-0199.1, 2016.

1146 Pinter, N., van der Ploeg, R.R., Schweigert, P. and Hoefler, G.: Flood magnification on the River Rhine.
1147 *Hydrological Processes*, 20(1), 147-164, 2006.

1148 Putman, W. M., and S.-J. Lin: Finite-volume transport on various cubed-sphere grids. *Journal of Computational*
1149 *Physics*, 227 (1), 55–78, 2007.

1150 Rantz, S.E.: Measurement and computation of streamflow: volume 2, computation of discharge (No. 2175).
1151 USGPO, 1982. Available at: <http://pubs.usgs.gov/wsp/wsp2175/pdf/WSP2175_voll1a.pdf>.

1152 Rayner, N.A., Parker, D.E., Horton, E.B., Folland, C.K., Alexander, L.V., Rowell, D.P., Kent, E.C. and Kaplan,
1153 A.: Global analyses of sea surface temperature, sea ice, and night marine air temperature since the late
1154 nineteenth century. *Journal of Geophysical Research: Atmospheres*, 108(D14), doi:10.1029/2002JD002670,
1155 2003.

1156 Stafford, Robert, T., Stafford disaster relief and emergency assistance act. *Public Law*, 10(30), 106-390, 2000.

1157 Scherrer, S.C., Fischer, E.M., Posselt, R., Liniger, M.A., Croci- Maspoli, M. and Knutti, R.: Emerging trends in
1158 heavy precipitation and hot temperature extremes in Switzerland. *Journal of Geophysical Research:*
1159 *Atmospheres*, doi:10.1002/2015JD024634, 2016.

1160 Schleifstein, M.: Louisiana Flood of 2016 resulted from '1,000-year' rain in 2 days, *NOLA*, viewed at 23 August
1161 2016, <http://www.nola.com/weather/index.ssf/2016/08/louisiana_flood_of_2016_result.html>.

1162 Sterl, A., Brink, H.V.D., Vries, H.D., Haarsma, R. and Meijgaard, E.V.: An ensemble study of extreme storm
1163 surge related water levels in the North Sea in a changing climate. *Ocean Science*, 5(3), 369-378, 2009.

1164 Strum, B.: Damage Grows from Louisiana Flood. *Wall Street Journal*, viewed at 23 August 2016,
1165 <<http://www.wsj.com/articles/damage-grows-from-louisiana-flood-1471803140>>.

1166 Taylor, K.E., Stouffer, R.J. and Meehl, G.A.: An overview of CMIP5 and the experiment design. *Bulletin of the*
1167 *American Meteorological Society*, 93(4), 485-498, 2012.

1168 Trambly, Y., Bouvier, C., Martin, C., Didon-Lescot, J.F., Todorovik, D. and Domergue, J.M.: Assessment of
1169 initial soil moisture conditions for event-based rainfall-runoff modelling. *Journal of Hydrology*, 387(3), 176-
1170 187, 2010.

1171 Van der Wiel, K., Kapnick S.B., Vecchi G.A., Cooke, W.F., Delworth T.L., Jia L., Murakami H., Underwood
1172 S., and Zeng F.: The resolution dependence of contiguous US precipitation extremes in response to CO2
1173 forcing. *J. Climate*, doi: 10.1175/JCLI-D-16-0307.1, 2016.

1174 Van Oldenborgh, G. J., Otto, F. E. L., Haustein, K., and Cullen, H.: Climate change increases the probability of
1175 heavy rains like those of storm Desmond in the UK – an event attribution study in near-real time, *Hydrol. Earth*
1176 *Syst. Sci. Discuss.*, 12, 13197-13216, doi:10.5194/hessd-12-13197-2015, in review, 2015.

1177 Van Oldenborgh, G. J., Philip, S., Aalbers, E., Vautard, R., Otto, F., Haustein, K., Habets, F., Singh, R., and
1178 Cullen, H.: Rapid attribution of the May/June 2016 flood-inducing precipitation in France and Germany to
1179 climate change, *Hydrol. Earth Syst. Sci. Discuss.*, doi:10.5194/hess-2016-308, in review, 2016.

1180 Van Vuuren, D.P., Edmonds, J., Kainuma, M., Riahi, K., Thomson, A., Hibbard, K., Hurtt, G.C., Kram, T.,
1181 Krey, V., Lamarque, J.F., Masui, T., Meinshausen, M., Nakicenovic, N., Smith, S., and Rose, S.: The
1182 representative concentration pathways: an overview. *Climatic change*, 109, 5-31, 2011.

1183 Vecchi, G.A., Fueglistaler, S., Held, I.M., Knutson, T.R., and Zhao, M.: Impacts of Atmospheric Temperature
1184 Changes on Tropical Cyclone Activity. *J. Climate* doi: 10.1175/JCLI-D-12-00503.1, 2013.

1185 Vecchi, G.A., and Soden. B.J.: Effect of remote sea surface temperature change on tropical cyclone potential
1186 intensity, *Nature*, 450, 1066-1070 doi:10.1038/nature06423, 2007.

1187 Vecchi, G.A., Delworth, T., Gudgel, R., Kapnick, S.B., Rosati, A., Wittenberg, A.T., Zeng, F., Anderson, W.,
1188 Balaji, V., Dixon, K. Jia, L., Kim, H-S, Krishnamurthy, L., Msadek, R., Stern, W.F, Underwood, S.D., Villarini,
1189 G., Yang, X., and Zhang, S.: On the seasonal forecasting of regional tropical cyclone activity. *J. Climate*,
1190 27(21), 7994-8016, 2014.

1191 Villarini, G., Goska, R., Smith, J.A. and Vecchi, G.A.: North Atlantic tropical cyclones and US flooding.
1192 *Bulletin of the American Meteorological Society*, 95(9), 1381-1388, 2014.

1193 Walsh, K., Camargo, S., Vecchi, G., Daloz, A., Elsner, J., Emanuel, K., Horn, M., Lim, Y.-K., Roberts, M.,
1194 Patricola, C., Scoccimarro, E., Sobel, A., Strazzo, S., Villarini, G., Wehner, M., Zhao, M., Kossin, J., LaRow,
1195 T., Oouchi, K., Schubert, S., Wang, H., Bacmeister, J., Chang, P., Chauvin, F., Jablonowski, C., Kumar, A.,
1196 Murakami, H., Ose, T., Reed, K., Saravanan, R., Yamada, Y., Zarzycki, C., Vidale, P., Jonas, J., Henderson, N.:
1197 Hurricanes and climate: the U.S. CLIVAR working group on hurricanes. *Bull. Amer. Meteorol. Soc.*
1198 doi:10.1175/BAMS-D-13-00242.1, 2015.

1199 Yang, X., Vecchi, G.A., Gudgel, R.G., Delworth, T.L., Zhang, S., Rosati, A., Jia, L., Stern, W.F., Wittenberg,
1200 A.T., Kapnick, S. and Msadek, R.: Seasonal predictability of extratropical storm tracks in GFDL's high-
1201 resolution climate prediction model. *J. Climate*, 28(9), 3592-3611, 2015.

1202 Zhang, W., Vecchi, G.A., Murakami, H., Delworth, T., Wittenberg, A.T., Anderson, W., Rosati, A.,
1203 Underwood, S., Harris, L., Gudgel, R., Lin, S.-J., Villarini, G., and Chen, J.-H.: Improved Simulation of
1204 Tropical Cyclone Responses to ENSO in the Western North Pacific in the High-Resolution GFDL HiFLOR
1205 Coupled Climate Model. *J. Climate*, doi:10.1175/JCLI-D-15-0475.1, 2016.

1206 Zhang, W., Leung, Y. and Fraedrich, K.: Different El Niño types and intense typhoons in the Western North
1207 Pacific. *Climate Dynamics*, 44(11-12), 2965-2977, 2015.